

### ACKNOWLEDGEMENTS

Sincere thanks and gratitude are expressed to Dr. C.K. Kwok and Dr. R. Cheng for their guidance, generous advice and encouragement at all times. The author is greatly indebted to them for providing a variety of experience in the laboratory of the Fluid Control Center and for the financial assistance received therefrom.

To Dr. S. Katz the author is grateful for the helpful discussions relating to fluid mechanics relevant to the present study. Thanks are also due to those who were directly or indirectly associated with the author during the course of the investigation.

## TABLE OF CONTENTS

### CHAPTER 1

### Page

#### LIQUID OPERATED OSCILLATOR: GENERAL REVIEW

1.1	Introduction	1
1.2	Diaphragm type Fluid Oscillator	1
1.2.1	Description and Operation Principle	1
1.3	Applications	4

### CHAPTER 2

#### FLUID BALL OSCILLATOR: THEORETICAL ANALYSIS

2.1	Introduction	6
2.2	Description and Operation Principle of the Ball Oscillator	6
2.3	Calculation Procedure Concept	7
2.4	Calculation of Time $t_1$	8
2.4.1	Main Factors Affecting Time $t_1$	8
2.4.2	Evaluation of Friction Factor Regions	9
2.4.3	Idealized Theoretical Model of the Slug Motion	10
2.4.3.1	Introduction and General Concept	10
2.4.3.2	Effect of Dissolved Air	12
2.4.3.3	Formulation of the Equation Governing the Slug Motion	14

## Table of Contents (continued)

	<u>Page</u>
2.4.3.4 Effect of the Body Force and General Remarks	17
2.4.4 Leakage Effect on the Frequency	19
2.4.4.1 Calculation of the Leakage Area	19
2.4.4.2 Calculation of the Accumulation Velocity	20
2.5 Calculation of Time $t_2$	28
2.5.1 Introduction	28
2.5.2 Calculation of the Travelling Distance	28
2.5.3 The Concept of the Mathematical Model	30
2.5.4 Range of Operation for the Mathematical Model	30
2.5.5 Forces Analysis Approach	31

## CHAPTER 3

### EXPERIMENTAL INVESTIGATIONS

3.1 Introduction	37
3.2 Components of the Prototype of the Oscillator	38
3.3 Verification of the Slug Motion and Ball Oscillation	39
3.4 Experimental Apparatus	40
3.5 Procedure	42

## CHAPTER 4

### DISCUSSION OF THE RESULTS

4.1 Introduction	44
------------------	----

## Table of Contents (continued)

	<u>Page</u>
4.2 Effect of the Initial Discharge Velocity	45
4.3 Effect of Tube Length	45
4.4 Effect of Oscillator Design, With or Without Leakage	46
4.5 Effect of the Angle $\delta$ of the Inner Ball-Housing	46
4.6 Effect of the Ball Material	47

## CHAPTER 5

### CONCLUSIONS AND RECOMMENDATIONS FOR FUTURE WORK

5.1 Conclusions	49
5.2 Recommendations for Future Work	50

REFERENCES	52
FIGURES	54
APPENDIX A: MIMIC Program for the Solution of the Forward and Reverse Slug Motion Equations.	100

APPENDIX B: FORTRAN Program for the Solution of the Mathematical Model.	102
---	-----

## LIST OF FIGURES

	Page
1. Cross-sectional view of fluid oscillator	55
2. Effect of vent tube geometry on frequency	56
3. Typical oscillator output pressure waveforms	57
4. General form of the ball oscillator	58
5. Friction factor and Reynolds number relationship (smooth pipes)	58
6. Moody chart for any type of commercial pipe	59
7. Linear approximation of the smooth pipes curve	60
8. Control volume for forward and reverse motion	61
9. Forward and reverse motion (without leakage)	62
10. Typical graphical solution of the MIMIC program solution	63
11. Effect of body force on time $t_1$ (without leakage)	64
12. Effect of body force on maximum forward slug displacement	65
13. Clearance area calculation	66
14. Forward and reverse motion (with leakage)	67
15. Relationship between discharge velocity and time $t_1$ (theoretical and experimental) $\bar{a} = 30^\circ$	68
16. Relationship between discharge velocity and time $t_1$ (theoretical and experimental) $\bar{a} = 25^\circ$	69
17. Relationship between discharge velocity and time $t_1$ (theoretical and experimental) $\bar{a} = 20^\circ$	70
18. Relationship between discharge velocity and maximum displacement (theoretical) $\bar{a} = 30^\circ$	71
19. Relationship between discharge velocity and maximum displacement (theoretical) $\bar{a} = 25^\circ$	72

20.	Relationship between discharge velocity and maximum displacement (theoretical) $\delta = 20^\circ$	73
21.	Forces analysis of the inside ball-housing of the oscillator	74
22.	Contraction coefficient curve.	75
23.	Time $t_2$ in millisec for angle $\delta = 30^\circ$	76
24.	Time $t_2$ in millisec for angle $\delta = 25^\circ$	77
25.	Time $t_2$ in millisec for angle $\delta = 20^\circ$	78
26.	Frequency of the oscillator, with leakage $\delta = 30$	79
27.	Frequency of the oscillator, with leakage $\delta = 25$	80
28.	Frequency of the oscillator, with leakage $\delta = 20$	81
29.	Frequency of the oscillator, without leakage	82
30.	Assembly drawing of the oscillator prototype	83
31.	Main outside body of the prototype	84
32.	Inner ball-housing with $\delta = 35^\circ$	85
33.	Inner ball-housing with $\delta = 30^\circ$	86
34.	Inner ball-housing with $\delta = 25^\circ$	87
35.	Inner ball-housing with $\delta = 20^\circ$	88
36.	Inner ball-housing with $\delta = 15^\circ$	89
37.	Inner ball-housing without leakage	90
38.	Locking nut	91
39.	Discharge tube with different length	92
40.	Relationship between the rotameter and the supply pressure	93
41.	Relationship between the supply pressure and the discharge velocity	94
42.	Typical pressure distribution at points 1 and 2	95

43.	Pressure distributions at points 1 and 2, $P_s = 20$ psig, $L = 2'$ , without leakage	96
44.	Pressure distributions at points 1 and 2, $P_s = 30$ psig, $L = 2'$ , without leakage	96
45.	Pressure distributions at points 1 and 2, $P_s = 45$ psig, $L = 2'$ , without leakage	97
46.	Pressure distributions at points 1 and 2, $P_s = 66$ psig, $L = 2'$ , without leakage	97
47.	Pressure distributions at points 1 and 2, $P_s = 35$ psig, $L = 1.5'$ , without leakage	98
48.	Pressure distributions at points 1 and 2, $P_s = 65$ psig, $L = 1.5'$ , without leakage	98
49.	Pressure distributions at points 1 and 2, $P_s = 65$ psig, $L = 2'$ , with leakage $\delta = 30^\circ$	99
50.	Pressure distributions at points 1 and 2, $P_s = 60$ psig, $L = 2'$ , with leakage $\delta = 30^\circ$	99

### LIST OF TABLES

	Page
Table 1 Numerical values for time $t_1$ and $x_{\max}$ ( $L = 24$ inches)	24
Table 2 Numerical values for time $t_1$ and $x_{\max}$ ( $L = 12$ inches)	24
Table 3 Numerical values for time $t_1$ and $x_{\max}$ ( $L = 6$ inches)	25
Table 4 Travelling distance for different cone angles	30
Table 5 Clearance area for different cone angles	31
Table 6 Different angles $b$ corresponding to different cone angle	35



## NOMENCLATURE

$\alpha$	Inner inclination of the ball-housing.
$A$	Cross-section area of the discharge tube.
$A_{cl}$	Clearance area.
$A_{ell}$	Ellipse area.
$\epsilon$	Cone angle of the ball-housing.
$C_c$	Coefficient of contraction.
$C_D$	Coefficient of discharge.
$C_K$	Constant.
$C_V$	Coefficient of velocity.
$d$	Inside diameter of the discharge tube.
$D$	Inside diameter of the ball-housing.
$D_b$	Ball diameter.
$f$	Friction factor.
$F_B$	Buoyant force.
$F_f$	Flow force.
$F_g$	Gravity force.
$F_s$	Suction force.
$g$	Gravitational acceleration.
$l$	Length of the discharge tube.
$m$	Mass of the ball.
$m_{air}$	Mass of the released air inside the cavity.
$P_a$	Atmospheric pressure.

$P_{air}$	Pressure of the air inside the cavity.
$P_c$	Pressure inside the cavity.
$P_s$	Supply pressure.
$P_v$	Vapor pressure.
$P_l$	Mean value of the pressure inside the ball-housing.
$r$	Radius of the ball.
$R_{air}$	Gas constant of air.
$R_e$	Reynolds number.
$t$	Time.
$t_{xmax}$	Time necessary for maximum forward slug displacement.
$t_1$	Time during which the ball remains on the hole.
$t_2$	Time required for moving the ball from one hole to the other.
$T$	Total time of one complete cycle.
$T_{air}$	Absolute air temperature.
$V_{acc}$	Accumulation velocity.
$V_c$	The volume of the cavity.
$V_o$	Initial discharge velocity.
$W_w$	Specific weight of the supply water.
$x$	Displacement of the slug.
$x_{max}$	Maximum forward slug displacement.
$y$	Distance from oscillator center line to discharge tube center line.
$Y$	Travelling ball distance.

$\alpha$	Angular acceleration of the ball.
$\beta$	Air release rate.
$\mu$	Coefficient of friction.
$\rho$	Density.
$\theta$	Inclination of the oscillator with the vertical axis.
$\tau_f$	Shear stress.

## CHAPTER 1

### LIQUID OPERATED OSCILLATOR

#### 1.1 INTRODUCTION

Major problems have limited the extent of work done on liquid operated low frequency oscillators. One such difficulty is that the wave propagation velocity in liquid is many times higher than in air; therefore, any liquid oscillator design using the wave propagation principle will result in a device with high oscillation frequencies. Furthermore, the incompressibility of liquids prohibits the use of fixed volume capacitors (the incompressibility of liquids necessitates the use of variable volume capacitors which add to the complexity as well as the physical dimensions of the system) [1], [2].

The following discussion [3], [4] presents the concept of a simple liquid operated low frequency oscillator: the diaphragm type fluid oscillator. The main operating principle of this oscillator depends on the inertia effect of the fluid in the discharge tube of the oscillator.

#### 1.2 DIAPHRAGM TYPE FLUID OSCILLATOR

##### 1.2.1 Description and Working Principle

A schematic cross-sectional view of the fluid oscillator is shown in Figure 1. The device consists of a supply nozzle that

directs flow into a receiver having a larger diameter than, and located concentric with, the supply nozzle. Between the receiver and the supply nozzle there is a small gap, called the ejector chamber, connected to the output line. The supply nozzle, receiver and the output line together act as an ejector system. The other end of the receiver connects to the seat chamber. Surrounding the seat chamber is the vent chamber connected to a vent tube. A diaphragm made of polyurethane closes the curtain area between the two chambers. A spring with a force adjusting screw is provided to keep the diaphragm in position. A spring retainer is placed between the diaphragm and the spring to make the motion of the diaphragm uniform.

Fluid at a supply pressure  $P_s$  enters the seat chamber, where the pressure is  $P_1(t)$ , through the supply nozzle of cross-sectional area  $A_n$ . There is no flow into the vent chamber while the diaphragm is closed. As the pressure  $P_1$  increases, it eventually causes the diaphragm to lift from the seat and to allow flow into the vent chamber, where the pressure is  $P_2(t)$ . The diaphragm continues to move upward as long as the forces on the diaphragm due to  $P_1$  and  $P_2$ , together with the inertial force due to the mass of the diaphragm, are greater than the downward force of the spring. During this phase of operation, the output channel, which is connected to the ejector chamber, is experiencing a negative pressure due to the venturi effect of the ejector system. At this point, the spring is being compressed, exerting a force which tends to close the diaphragm against its seat. Furthermore, it can be seen that as maximum flow

into the vent chamber is achieved, the fluid velocity between the diaphragm and the seat is at its highest value and, according to the Bernoulli's relation, pressure will decrease correspondingly. The reduction in static pressure in that region causes the diaphragm to start moving downwards. When this happens, the cross-sectional flow area between the seat and the diaphragm will be reduced. This will decrease the flow into the vent chamber and further reduce its pressure. This reduction of pressure causes an additional downward deflection of the diaphragm resulting in a further decrease of flow into the vent chamber. Eventually, the diaphragm will snap onto the seat blocking the entire flow into the vent chamber. However, before the snap closing of the diaphragm, the whole column of liquid within the vent tube has been accelerated. Due to the inertia of the liquid, the sudden closing of the diaphragm cannot produce an immediate stoppage of the moving liquid within the vent tube. The liquid in the tube continues to move, thus creating a strong vacuum within the vent chamber which pulls the diaphragm further downwards against the seat. This effect creates an even tighter closing of the diaphragm against its seat and diverts all the supply flow into the output line. This process produces a strong positive oscillating phenomenon with a high output pressure recovery.

As soon as the inertia of the liquid in the vent tube has expired, the pressure in the vent chamber returns from sub-ambient to ambient. When the pressure in the vent chamber returns to normal ambient pressure, the total force acting on the diaphragm will be

high enough to push the diaphragm upwards against the spring force. Once the diaphragm starts to open, the flow entering the vent chamber will again build up. This build up of pressure thus causes a further deflection of the diaphragm. When this occurs, the output pressure at the outlet drops immediately and reaches a sub-ambient pressure caused by the entire supply flow entering the vent chamber through the receiver tube.

Since the inertia effect of the column of liquid in the vent tube is responsible for the oscillation phenomenon, the variation in tube geometry will change the inertia effect thus causing a corresponding change in the oscillation frequency. Figure 2 [3], [4] illustrates the effect of vent tube geometry on the frequency. Generally, increases in oscillation frequency can be achieved by increasing vent tube diameter, decreasing vent tube length, decreasing vent and seat diameters and increasing spring stiffness and initial spring force.

Typical oscillator output pressure waveforms [2] are shown in Figure 3. An analytical study of this oscillator was carried out using the linear graph technique as described in references [3],[4], in an attempt to understand the effects of various design parameters which affect the operation of the oscillator.

### 1.3 APPLICATIONS.

The operation as well as the construction of the fluid diaphragm oscillator are relatively simple. This device appears to

offer exciting performance characteristics and excellent reliability due to lack of moving parts. These advantages make the fluid oscillator particularly attractive for various applications such as a lawn sprinkler [5], pulsating dental syringe, oscillating showerhead [2], and pulsating car wash [1].



## CHAPTER 2

### FLUID BALL OSCILLATOR: THEORETICAL APPROACH

#### 2.1 INTRODUCTION

In this chapter, a new type of a liquid operated low frequency oscillator, which is the subject of the thesis, is introduced. The operating principle of this type also depends upon the inertia effect of the fluid in the discharge tube. This oscillator has many advantages such as simple design and construction, reliable operation and does not need much maintenance. Applications of the ball oscillator include an oscillating showerhead, a pulsating car wash as well as other water cleaning devices. The main objective of this chapter is to present the concept of the new liquid operated low frequency oscillator.

#### 2.2 DESCRIPTION AND OPERATION PRINCIPLE OF THE BALL OSCILLATOR

A general form of the oscillator consists of a housing, of diameter  $D$ , having a fluid inlet channel connected to a pressure source as shown in Figure 4. At the bottom of this housing, there are two outlet discharge tubes of inner diameter  $d$ , and a ball inside the housing controls the water discharge through these tubes. The discharge tube lengths can be easily varied by connecting additional tubing at the ends of the original tubes.

When the ball blocks the inlet hole of one of the two dis-

charge tubes of the oscillator, the column of water already inside the blocked tube continues to move downwards due to the inertia of the fluid. Thus a strong vacuum is developed in the cavity between the ball and the downward moving water column. The liquid slug inside the tube continues to move downwards until the inertial energy is dissipated and the velocity is reduced to zero. At this point, the fluid slug starts to return towards the ball, owing to the difference between the vapor pressure inside the cavity and the outside ambient pressure, until it reaches the upper end of the discharge tube. At this stage of operation, the total pressure inside the housing is large enough to push the ball to the inlet of the other discharge tube and the same procedure is then repeated.

Since the inertia effect of the column of liquid in the discharge tube is responsible for the forward and reverse motion of the liquid slug, any variation in tube geometry (diameter and length) will affect the time interval between the ball-valve closure and the collapse of the cavity.

The secondary parameters affecting the total time for one complete ball oscillation cycle are: the inlet water temperature, discharge tube material, inside geometry of the ball-housing and the size and weight of the ball.

### 2.3 CALCULATION PROCEDURE CONCEPT

The total time necessary for one complete cycle may be calculated as follows:

7

$T = 2(t_1 + t_2)$ ; where

$T$  = period of oscillation.

$t_1$  = time during which the ball remains on the hole.

$t_2$  = time required for moving the ball from one hole to the other.

## 2.4 CALCULATION OF TIME $t_1$

### 2.4.1 Main Factors Affecting the Time $t_1$

1. Inlet water temperature. The supply water temperature affects the vapor pressure, the specific weight of the water and the viscosity.
2. Supply pressure. Experimental and theoretical results have shown that the supply pressure is the most important factor affecting the oscillator frequency. This is because an increase in pressure leads to an increase in the discharge velocity.
3. The length and diameter of the discharge tube. The length of the discharge tube has been found to be a very important factor. The diameter of the discharge tube also affects the time  $t_1$  but not to the same degree as the discharge tube length.
4. Tube material. The friction factor depends on the tube material and its surface finish. For the case of flow in very smooth pipes, values of friction factor  $f$  vary with Reynolds number  $R_e$ , as shown in the curve of

Figure 5. It may be seen that this curve never becomes horizontal, which shows that the fluid properties influence the flow throughout the entire range of Reynolds number. Glass pipes or very smooth-drawn tubing or reasonably smooth pipes would fall into this category [6].

In the case under study, the prototype ball oscillator was manufactured from plexi-glass and hence the "smooth pipes" curve, shown in Figure 6 was chosen for the calculation of the time  $t_1$ .

Since the velocity inside the tube varies with time (starting from the initial discharge velocity until zero), the value of the friction factor is not constant during the time period  $t_1$ .

#### 2.4.2 Evaluation of Friction Factor Regions

The relationship between Reynolds number  $R_e$  and the friction factor for any type of commercial pipe is shown in Figure 6 [7],[8]. Figure 7 illustrates the mathematical relationships between Reynolds number and the friction factor and their regions of validity given by previous investigators [9],[10]. Those mathematical relationships may be expressed as follows:

$$\text{for } R_e < 2 \times 10^3; f = 64/R_e; \text{ valid in region (A)} \quad (1)$$

$$\text{for } 2 \times 10^3 < R_e < 4 \times 10^3; \frac{1}{\sqrt{f}} = -2.1 \log \left( \frac{e/d}{3.7} + \frac{2.51}{R_e \sqrt{f}} \right);$$

valid in region (B) (2)

$$\text{for } R_e > 4 \times 10^3; \frac{1}{\sqrt{f}} = 2 \log(R_e \sqrt{f}) - .80; \text{ valid in region (C)} \quad (3)$$

where  $R_e$  is the Reynolds number,

$f$  the friction factor,

$e/D$  the relative roughness.

The mathematical expressions of the friction factor given by Equations (1), (2) and (3) may be simplified for ease of computational programming as shown in Figure 7. In this figure, the curve in regions B and C, is approximated by two empirical straight line equations. The results of the friction factor obtained by using the latter equations have proved to be sufficiently accurate [9], [10] [11]. The two straight lines intersect approximately at a Reynolds number equal to  $1 \times 10^5$ . According to Figure 7, the friction factor regions may be expressed as follows [11], [12], [14]

$$\text{for } R_e < 2 \times 10^3; f = 64/R_e; \text{ valid in region (I)} \quad (4)$$

$$\text{for } 2 \times 10^3 < R_e < 1 \times 10^5; f = .3164/R_e^{.25}; \text{ valid in region (II)} \quad (5)$$

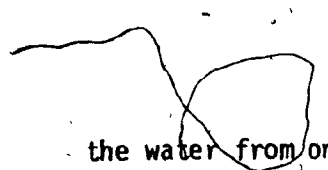
$$\text{for } R_e > 1 \times 10^5; f = .1840/R_e^{.20}; \text{ valid in region (III)} \quad (6)$$

Equations (4), (5) and (6) are employed in this report to calculate the variation of the friction factor for varying values of  $R_e$ .

### 2.4.3 Idealized Theoretical Model of the Slug Motion

#### 2.4.3.1 Introduction and General Concept

Figure 8 shows a generalized model used to investigate the slug motion in an inclined tube. The control volume consists of a short length,  $\ell$ , of rigid wall tube and a ball-valve which blocks



the water from one of the two tubes of the oscillator. Each tube has an inside diameter,  $d$ , and is inclined at angle  $\theta$  to the vertical axis. With the ball-valve fully open (Figure 8,a) the water flows through the tube at initial velocity  $V_0$ . If the ball-valve is suddenly closed (Figure 8,b), the column of water already inside the tube continues to move due to the inertia of the fluid, i.e., sudden closing of the ball-valve cannot produce an immediate stoppage of the moving liquid. Thus a cavity of growing length  $x$ , is developed between the downstream ball-valve side and the forward moving water column. The pressure inside the cavity is made up of two components one of which is the vapor pressure of the liquid,  $P_v$ . However, air dissolved in the water enters the cavity and so raises the cavity pressure slightly. Thus the pressure inside the cavity is the vapor pressure of the water plus the partial pressure of the air released out of the water in the neighborhood of the cavity. At the discharge end of the tube the pressure,  $P_a$ , is atmospheric pressure.

The following analysis is based on a theory referred to as the "rigid column" theory in which the liquid is assumed to be incompressible [13]. The coefficient of friction,  $f$ , for unsteady flow will be assumed to be essentially the same as for steady flow [13]. Actually, the velocity at any instant varies slightly along the discharge tube due to pressure waves. However, since the tube length is short, the wave propagation time is much less than the total time taken by the water column to move forward and return. Hence the effect of pressure waves on velocity is neglected. One purpose of

the following analysis is to determine the time between the ball-valve closure and the collapse of the cavity.

#### 2.4.3.2 Effect of Dissolved Air

The water column contains dissolved air which comes out of solution and enters the cavity [15],[16],[17]. The pressure inside the cavity is equal to the sum of the vapor pressure and the partial pressure of the air released from the water. Several previous models for cavity pressure consider the effect of the dissolved air [15],[16]. When the model assumes the rate at which air comes out of solution [15] and the universal gas law is used, the cavity pressure may be expressed as:

$$P_c = P_v + P_{air}$$

$$P_{air} \times V_c = m_{air} \cdot R_{air} \cdot T_{air}$$

$$P_{air} = \frac{m_{air} \cdot R_{air} \cdot T_{air}}{V_c} = \frac{\beta \cdot t(R_{air} \cdot T_{air})}{(\pi d^2/4) \cdot x}$$

therefore

$$P_c = P_v + \frac{\beta \cdot t(R_{air} \cdot T_{air})}{(\pi d^2/4) \cdot x}$$

where

$P_{air}$  = the pressure of the air in the cavity at the time  $t$ .

$V_c$  = the volume of the cavity at time  $t$ .

$m_{air}$  = the mass of air in the cavity at time  $t$ .

$R_{air}$  = the gas constant of air.

$T_{air}$  = the temperature of the air within the cavity, which is assumed constant and equal to the water temperature.

$\beta$  = air release rate from the water.

$d$  = inner diameter of the discharge tube.

$x$  = length of the cavity at time  $t$ .

The rate at which dissolved air enters the cavity,  $\beta$ , is assumed equal to  $20 \times 10^{-6}$  kg/sec. This is close to the value recommended in [15], [18] for the water column separation and cavitation in short tubes. The effect of the dissolved air becomes progressively more significant as the initial discharge velocity is lowered. When the initial velocity is low, the cavity volume remains small so that the air entering causes a higher cavity pressure. This acts to move the column further in the forward direction.

During the reverse slug motion (cavity collapse), no air is allowed back into the solution [16], [18]. Thus, the mass of air in the cavity is fixed at  $\beta \cdot t_{xmax}$  and the cavity pressure is:

$$P_c = P_v + \frac{\beta \cdot t_{xmax} (R_{air} \cdot T_{air})}{(\pi d^2 / 4) \cdot x}$$

where  $t_{xmax}$  is the time necessary for maximum forward slug displacement.

For simplicity, the cavity pressure may be assumed constant and equal to the vapor pressure, i.e.  $\beta = 0$ . This assumption is reasonable when the initial velocity is high. Then, the cavity volume is large and the dissolved air has less effect [18]:



### 2.4.3.3 Formulation of the Equation Governing the Slug Motion

The resultant force acting on a control volume is equal to the time rate of increase of linear momentum within the control volume plus the net efflux of linear momentum from the control volume [10]. The linear momentum equation is given by [9],[10], [11],[19]:

$$\Sigma F = \int_{\text{control surface}} \rho \cdot V \cdot V \cdot dA + \frac{\partial}{\partial t} \int_{\text{control volume}} \rho \cdot V \cdot dv \quad (7)$$

As the time  $t$  is the only independent variable, the partial differentiation may be replaced by total differentiation. For this special case under study we have:

$V$  the velocity is not a function of the area  $A$ .

$dv$  the element of volume equal to  $A(l-x)$ .

$V \cdot dA = 0$ , where there is no inflow or outflow at the left side of the control volume under study.

$$\therefore \Sigma F = \int_{C.S.} \rho \cdot V \cdot V \cdot dA + \frac{d}{dt} \int_{C.V.} \rho \cdot V \cdot dA \cdot (l-x)$$

$$\Sigma F = \rho \cdot A \cdot V^2 + \rho A \frac{d}{dt} V(l-x) \quad (8)$$

since  $V = \frac{dx}{dt}$ , Equation (8) may be rewritten as follows:

$$\Sigma F = \rho A \left[ \left( \frac{dx}{dt} \right)^2 + \frac{d}{dt} \left( \frac{dx}{dt} \right) (l-x) \right]$$

$$\Sigma F = \rho A \left[ \left( \frac{dx}{dt} \right)^2 + (l-x) \cdot \frac{d^2 x}{dt^2} + \left( \frac{dx}{dt} \right) \cdot \frac{dx}{dt} \right]$$

$$\Sigma F = \rho A \left[ \left( \frac{dx}{dt} \right)^2 + (l-x) \frac{d^2 x}{dt^2} - \left( \frac{dx}{dt} \right)^2 \right]$$

$$\Sigma F = \rho \cdot A \cdot (l-x) \cdot \frac{d^2 x}{dt^2} = \text{density} \times \text{area} \times \text{slug length} \times \text{acceleration}$$

or Newton's second law of motion. (9)

The left hand side of Equation (7) is:

$$\Sigma F = (P_c - P_a)A - \tau_f(\pi d)(l-x) + \rho A(l-x) g \cos \theta \quad (10)$$

where

$$P_c = \text{cavity pressure} = P_v + \frac{\beta \cdot t(R_{\text{air}} \cdot T_{\text{air}})}{(\pi d^2/4) \cdot x}$$

$P_a$  = atmospheric pressure

$A$  = cross-sectional area of the tube

$d$  = inner tube diameter

$l$  = tube length

$\tau_f$  = shear stress

$\rho$  = density of supply water

$(P_c - P_a)A$  = pressure force

$\tau_f(\pi d)(l-x)$  = shear force

$\rho A(l-x) g \cos \theta$  = body force.

$$\text{Since } A = \pi d^2/4 \text{ and } \tau_f = \frac{1}{8} f \cdot \rho \cdot \left( \frac{dx}{dt} \right)^2 \quad [11]$$

Substitution of the above values of  $A$  and  $\tau_f$  in Equation (10) yields:

$$\Sigma F = (P_c - P_a) \frac{\pi d^2}{4} - \frac{1}{8} f \cdot \rho \cdot \left( \frac{dx}{dt} \right)^2 \cdot \pi d(l-x) + \rho \frac{\pi d^2}{4} (l-x) g \cos \theta \quad (11)$$

From Equations (9) and (10), we obtain the following:

$$(P_c - P_a) \frac{\pi d^2}{4} - \frac{1}{8} f \cdot \rho \cdot \left(\frac{dx}{dt}\right)^2 \cdot \pi d(l-x) = \rho \frac{\pi d^2}{4} (l-x) \left[ \frac{d^2 x}{dt^2} - g \cos \theta \right]$$

$$(P_c - P_a)d - \frac{1}{2} f \cdot \rho \cdot \left(\frac{dx}{dt}\right)^2 \cdot (l-x) = \rho \cdot d \cdot (l-x) \left[ \frac{d^2 x}{dt^2} - g \cos \theta \right]$$

$$\frac{(P_c - P_a)}{\rho(l-x)} - \frac{1}{2d} \cdot f \cdot \left(\frac{dx}{dt}\right)^2 = \frac{d^2 x}{dt^2} - g \cos \theta$$

Rearranging,

$$\frac{d^2 x}{dt^2} + \frac{1}{2d} \cdot f \cdot \left(\frac{dx}{dt}\right)^2 - g \cos \theta = \frac{1}{\rho(l-x)} (P_v + \frac{4\beta \cdot t \cdot R_{air} \cdot T_{air}}{\pi d^2 \cdot x} - P_a) \quad (12)$$

Equation (12) represents the general solution for the slug dynamics during the forward motion of time  $t_1$  with the following initial conditions:

at  $t = 0$ ,  $x = 0$  and  $\frac{dx}{dt} = V_0$  = initial discharge velocity.

and at  $x = x_{max}$  at  $\frac{dx}{dt} = 0$ . (13)

The reverse slug motion, according to the control volume shown in Figure 8 is similarly found to be:

$$(P_c - P_a) \frac{\pi d^2}{4} + \frac{1}{8} f \cdot \rho \cdot \left(\frac{dx}{dt}\right)^2 \cdot \pi d(l-x_{max}) = \rho \cdot \frac{\pi d^2}{4} \cdot (l-x_{max}) \left[ \frac{d^2 x}{dt^2} - g \cos \theta \right]$$

Rearranging,

$$\frac{d^2 x}{dt^2} - \frac{1}{2d} \cdot f \cdot \left(\frac{dx}{dt}\right)^2 - g \cos \theta = \frac{1}{\rho(l-x_{max})} (P_v + \frac{4\beta \cdot t_{x_{max}} \cdot R_{air} \cdot T_{air}}{\pi d^2 \cdot x} - P_a) \quad (14)$$

where:  $t_{x_{\max}}$  = time necessary for maximum forward slug displacement.

$x_{\max}$  = maximum forward slug displacement.

Equation (14) represents the general solution for the slug dynamics during the reverse motion of time  $t_1$  with the following initial conditions:

$$\text{at } t = 0, \quad x = x_{\max} \text{ and } \frac{dx}{dt} = 0 \quad (15)$$

The value of the friction factor,  $f$ , varies with the velocity variation and may be calculated, for the solution of Equations (12) and (14), by using the Equations (4), (5) or (6) as the case may be. Figure 9 illustrates the forward motion and the reverse motion of the slug during the time  $t_1$ . This motional behaviour has been confirmed by taking motion pictures using a high speed camera (4000 frames per second).

#### 2.4.3.4 Effect of the Body Force on Time $t_1$ and General Remarks

The general equations of the slug motion during the time  $t_1$ , may be solved together by using the MIMIC language technique. Appendix A shows the details of the MIMIC program. Figure 10 illustrates the typical graphical solution of Equations (12) and (14). This figure shows the relationships between the time  $t$ , in milliseconds, the forward and reverse slug motion, the velocity variation, the Reynolds number and the friction factor variation. The maximum forward slug displacement and the time  $t_1$  may be obtained as shown in Figure 10.

This program is useful for different working water temperatures (this is done by putting into the main program, the values of the vapor pressure, the density of the water and the viscosity, corresponding to the supply water temperature), different tube length and diameter, and various values of initial discharge velocity.

The computer solution has been carried out for  $\theta = 0^\circ$  (Case a, where the discharge is in the downward direction), for  $\theta = 180^\circ$  (Case c, where the discharge is in the upward direction) and finally for  $\theta = 90^\circ$  (Case b, where the discharge is in the horizontal direction). Figure 11 represents the theoretical and experimental results obtained for the time  $t_1$  versus different initial discharge velocities, for various tube lengths and angle  $\theta$ . Figure 12 represents the theoretical results obtained for the maximum forward slug displacement versus different initial discharge velocities, for various tube lengths and angles of inclination  $\theta$ . From Figures 11 and 12 it may be noticed that for small tube lengths (approximately less than 3 inches) the time  $t_1$  and the maximum forward slug displacement are relatively small, thus preventing proper oscillation. This behaviour has been experimentally verified by using an oscillator prototype with very short tube lengths. Figures 11 and 12 also show that, for oscillators such as the prototype, the angle of inclination,  $\theta$ , of the tube with the vertical axis has only a small effect on the total time  $t_1$ . The analysis of Figures 11 and 12 shows that the total time between the ball-valve closure and subsequent

cavity collapse depends mainly on two parameters. The first parameter is the initial velocity of the water in the tube prior to closing. The second parameter is the length of the discharge tube. As a result of this insensitivity to variation in  $\theta$ , the effect of body force  $[pA(l-x)g \cos \theta]$  on time  $t_1$  may be neglected in the case of an oscillator such as the prototype, especially when the discharge tube length is short and the initial velocity is small. For a tube length equal to 3 inches, the body force effect is experimentally found to be negligible and for a tube length equal to 24 inches, the variation in the frequency was found to be only  $\pm 1$  to 1.5 Hertz.

Consequently, Equations (12) and (14) which govern the forward and reverse slug motions respectively, may be rewritten as follows:

$$\frac{d^2x}{dt^2} + \frac{1}{2d} \cdot f \cdot \left(\frac{dx}{dt}\right)^2 = \frac{1}{\rho(l-x)} \left( P_v + \frac{4\beta \cdot t \cdot R_{air} \cdot T_{air}}{\pi d^2 \cdot x} - P_a \right) \quad \text{forward motion}$$

$$\frac{d^2x}{dt^2} - \frac{1}{2d} \cdot f \cdot \left(\frac{dx}{dt}\right)^2 = \frac{1}{\rho(l-x_{max})} \left( P_v + \frac{4\beta \cdot t_{xmax} \cdot R_{air} \cdot T_{air}}{\pi d^2 \cdot x} - P_a \right) \quad \text{reverse motion}$$

#### 2.4.4. Leakage Effect on the Frequency

##### 2.4.4.1 Calculation of the Leakage Area

The lower part of the ball-housing has a conical shape. The upper end of each discharge tube intersects with the ball-housing in an elliptical section. The two axes of the ellipse are the major axis,  $d/\cos a$ , and the minor axis  $d$  as shown in Figure 13, where angle  $a$  is the inner housing inclination and  $d$  the inner tube diameter. The area of the ellipse is given by:

$$A_{ell} = \frac{\pi}{4} \times \frac{d}{\cos a} \times d = \frac{\pi d^2}{4 \cos a}$$

When the ball, with diameter  $D_b$ , stays on the hole, it does not fully close all of the elliptical intersection of the upper end of the discharge tube. Only a circular area equal to  $\pi d^2/4$  prevents the water from flowing through the discharge tube as shown in Figure 13. Consequently, the difference in area between the elliptical section and the circular section represents the leakage area, i.e.,

$$A_{cl} = \frac{\pi d^2}{4 \cos a} - \frac{\pi d^2}{4} = \left(\frac{\pi d^2}{4}\right) \left(\frac{1 - \cos a}{\cos a}\right) \quad (16)$$

It must be noted that the clearance area depends only on the tube inner diameter  $d$  and on the inner housing inclination, as seen in Equation (16). The ball diameter has no effect on the clearance area.

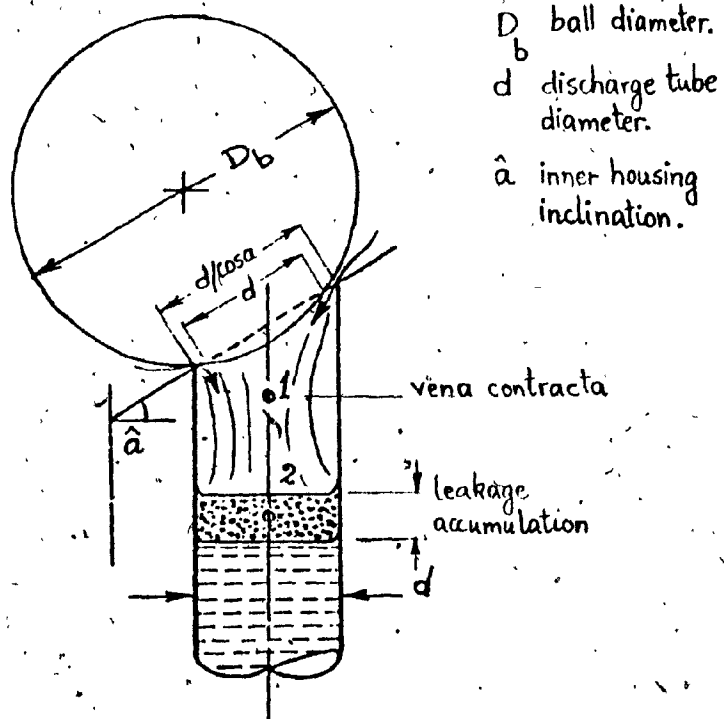
Due to the presence of this leakage area, a certain amount of fluid is accumulated on the top of the slug, thus affecting the displacement  $x$  and consequently reducing the time  $t_1$ . Figure 14 illustrates the forward and reverse motion of the slug during the time  $t_1$ , with the leakage accumulation on the top of the slug.

#### 2.4.4.2 Calculation of the Accumulation Velocity $V_{acc}$

An attempt, based on the principles of fluid mechanics to analyse the effect of leakage on the oscillation was carried out without success. Relevant literature pertaining to this case which represents an orifice with a liquid inlet flow and a vapor outlet

flow was found to be scarce.

The following figure represents the ball position while blocking the hole during the time  $t_1$ , and the amount of leakage accumulated on the top of the slug.





The actual case under study represents a complex phenomenon of an orifice with a liquid inlet flow and a vapor outlet flow, i.e., liquid to vapor orifice type.

Since no experimental data is available for such a case (liquid to vapor flow across an orifice), the accumulation velocity on the top of the slug may be represented empirically by the following equations:

$$V_{acc} = .542071 \sqrt{\Delta P} \text{ ft/sec; for } \hat{c} = 120^\circ \text{ } (\hat{a} = 30^\circ)$$

$$V_{acc} = .37428 \sqrt{\Delta P} \text{ ft/sec; for } \hat{c} = 130^\circ \text{ } (\hat{a} = 25^\circ)$$

$$V_{acc} = .23984 \sqrt{\Delta P} \text{ ft/sec; for } \hat{c} = 140^\circ \text{ } (\hat{a} = 20^\circ)$$

where,

$$\Delta P = P_s - P_c$$

$P_s$  = supply pressure

$P_c$  = cavity pressure

The best correlation between experimental and theoretical results for time  $t_1$  and maximum forward slug displacement,  $x_{\max}$ , for the case with leakage was obtained when using the previous empirical relationships for calculating the accumulated velocity.

In order to analyse such a complex leakage phenomenon (liquid to vapor flow), actual experimental tests and measurements inside the cavity during time  $t_1$  would have to be done. Such measurements need very sensitive techniques which are beyond the scope of this work.

Figure 10 illustrates the typical graphical solution for the relationships between the time  $t$ , in milliseconds, the forward and reverse slug displacement, the velocity variation, the Reynolds number and the friction factor variation. Clearly both the time  $t_1$  and the maximum forward slug displacement are less in the case with leakage than in the case without leakage. Figures 15, 16 and 17 illustrate the theoretical and experimental results for the relationship between the time  $t_1$  and the initial velocity  $V_0$  for different

tube lengths with different inclination angles  $\hat{\alpha}$  of  $30^\circ$ ,  $25^\circ$  and  $20^\circ$  respectively. Furthermore, Figures 18, 19 and 20 illustrate the theoretical results for the relationship between the maximum slug forward displacement,  $x_{\max}$ , and the initial velocity for different tube lengths with different inclination angles  $\hat{\alpha}$  of  $30^\circ$ ,  $25^\circ$  and  $20^\circ$  respectively.

Tables 1, 2 and 3 give some numerical values for the time  $t_1$  and the maximum forward slug displacement for different tube lengths (24, 12 and 6 inches) with leakage and without leakage. Those values are for an initial discharge velocity of 22 ft/sec and a supply water temperature of  $40^\circ\text{F}$ .

Cone Angle $\hat{\alpha}$	With Leakage			No Leakage
	$120^\circ$	$130^\circ$	$140^\circ$	$120^\circ$
Time $t_1$ , millisec	58.80	61.90	63.20	76.50
Max. Displ., inch	3.40	3.67	3.83	4.33

$L = 24''$

TABLE 1

Cone Angle $\hat{\alpha}$	With Leakage			No Leakage
	$120^\circ$	$130^\circ$	$140^\circ$	$120^\circ$
Time $t_1$ , millisec	28.00	30.80	32.40	39.50
Max. Displ., inch	1.55	1.86	2.04	2.38

$L = 12''$

TABLE 2

Cone angle $\epsilon$	With Leakage			No Leakage
	120°	130°	140°	120°
Time $t_1$ , millise	13.40	15.50	16.375	20.50
Max. Displ., inch	.72	.934	1.056	1.25

L = 6"

TABLE 3

From the above Tables, it can be seen that both time  $t_1$  as well as the maximum forward slug displacement increase as the cone angle  $\epsilon$  increase. Furthermore, the Tables show that the maximum possible values for  $t_1$  and  $x_{\max}$  may be obtained when using the no-leakage inner ball-housing. Likewise, as the discharge tube length increases, both time  $t_1$  and  $x_{\max}$  increase.

The following numerical example gives a general idea on the accumulation velocity, accumulation rate and the amount of leakage. Therefore, for an initial discharge velocity of 22 ft/sec, a discharge tube length of 12 inches, and a cone angle of 120°,  $v_{\text{acc}}$  may be calculated as follows:

$$v_{\text{acc}} = 4.965 \text{ ft/sec} \approx .05958 \text{ in/millise}$$

the accumulation rate = velocity  $\times$  area

$$= .05958 \pi \times .25 \times .25 / 4 = .00292463 \text{ in}^3 / \text{millisec}$$

$$= 2.924 \text{ in}^3 / \text{sec}$$

the amount of accumulation =  $V_{acc} \times \text{time}$

$$= .05958 \times 28 = 1.66824 \text{ inch.}$$

For this case, the percentage of accumulation to the total length is  $1.66824 / 12 = 13.902\%$  and this accumulation reduces time  $t_1$  from 39.5 millisec without leakage to about 28.00 millisec with leakage. Under the same conditions ( $V_0 = 22 \text{ ft/sec}$ ,  $\hat{c} = 120^\circ$ ) for a tube length of 24 inches, the amount of accumulation is  $.05958 \times 58.8 = 3.5003 \text{ inch}$ , hence the accumulation percentage is  $14.59\%$  and this accumulation reduces time  $t_1$  from 76.5 millisec without leakage to about 58.8 millisec with leakage.

The accumulation velocity depends basically on angle  $\hat{a}$  and on the supply pressure, i.e., on the initial discharge velocity. The tube length has no effect on the accumulation velocity. Practically, the ball is not exactly spherical. Also, the nominal dimensions of the discharge hole seat (the ellipse section) may change slightly with time because the inner ball-housing is manufactured from relatively soft material (plexi-glass). Due to these reasons, the accumulation velocity may vary during the operation.

The accumulation velocity may be represented empirically by the following procedure:

therefore,

$$V_{acc} = .542071 \sqrt{\Delta P} \text{ ft/sec ; for } \epsilon = 120^\circ (\alpha = 30^\circ)$$

$$V_{acc} = .37428 \sqrt{\Delta P} \text{ ft/sec ; for } \epsilon = 130^\circ (\alpha = 25^\circ)$$

$$V_{acc} = .23984 \sqrt{\Delta P} \text{ ft/sec ; for } \epsilon = 140^\circ (\alpha = 20^\circ)$$

Thus, from the previous study and analysis we may summarize the following points:

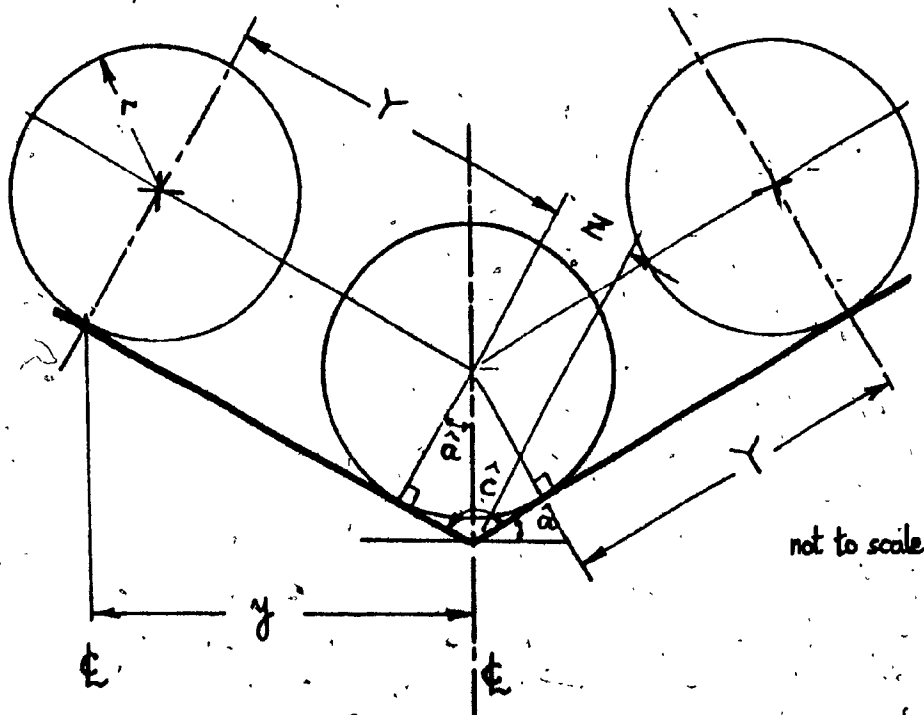
1. The two main parameters affecting time  $t_1$  and  $x_{max}$  are the initial discharge velocity (or the supply pressure) and the discharge tube length. As these two factors increase, both time  $t_1$  and  $x_{max}$  increase and vice versa.
2. The secondary parameter influencing time  $t_1$  and  $x_{max}$  is the cone angle of the inner ball-housing. As the cone angle increases, time  $t_1$  and  $x_{max}$  increase slightly.
3. The higher possible values of  $t_1$  and  $x_{max}$  are attained when using the no-leakage inner ball-housing.
4. Increasing the roughness of the discharge tube, i.e. increasing the friction factor, will result in an increase in the friction force, hence time  $t_1$  and  $x_{max}$  may decrease.
5. Increasing the water supply temperature will increase the vapor pressure inside the cavity. This results in moving the column of water further in the forward direction thereby increasing the time  $t_1$  and  $x_{max}$  slightly. This phenomenon has been verified experimentally in the laboratory by using a hot water supply.

## 2.5 CALCULATION OF TIME $t_2$

### 2.5.1 Introduction

The time,  $t_2$  may be defined as the time necessary for the ball to move from one discharge hole to the other. The distance travelled by the ball during this time is called the travelling distance. It is assumed that the ball rolls along the inner bottom surface of the ball-housing until it reaches the opposite discharge hole. That is, the ball does not jump from one hole to the other through the water inside the ball-housing. This assumption has been verified by experiments using high speed photography.

### 2.5.2 Calculation of the Travelling Distance



The above figure represents the ball motion along the inner surface of the ball-housing from one hole to the other. It has been assumed that the ball is already outside the seat of the hole and that the time necessary for such small shift may be neglected in comparison to time  $t_2$ . From the figure, we may calculate the travelling distance,  $2Y$ , as follows:

$$\tan a = Z/r \quad ; \quad Z = r \tan a$$

$$\cos a = \frac{y}{Y+Z} \quad ; \quad y = Y \cos a + Z \cos a \quad ; \quad Y \cos a = y - Z \cos a$$

$$Y = \frac{y - Z \cos a}{\cos a} = \frac{y}{\cos a} - Z$$

$$Y = \frac{y}{\cos a} - r \tan a = \frac{y}{\cos a} - \frac{r \sin a}{\cos a} = \frac{y - r \sin a}{\cos a}$$

$$\text{travelling distance } 2Y = \frac{2(y - r \sin a)}{\cos a}$$

where  $a$  inner inclination of the ball-housing

$r$  radius of the ball

$y$  distance from oscillator center-line to discharge tube center line.

Table 4 represents the distance  $Y$  for different cone angles, calculated for the oscillator model used in the experimental work, where the distance  $y = .25$  inch and the ball diameter  $D_b = 2r = 5/8$  inch.



Angle $\alpha$	15°	20°	25°	30°	35°
Cone Angle $\beta$	150°	140°	130°	120°	110°
Y mm	4.447	3.868	3.305	2.749	2.194

TABLE 4

### 2.5.3 The Concept of the Mathematical Model

In this study, a mathematical model for calculating the time  $t_2$  is introduced. The mechanism and the fundamental properties of oscillation are investigated analytically using this mathematical model (lumped parameter) and the validity of the model for calculating time  $t_2$  is confirmed experimentally.

### 2.5.4 Range of Operation for the Mathematical Model

This mathematical model is applied for the range  $150^\circ > \beta > 110^\circ$ . When the cone angle  $\beta$  is equal to or less than  $110^\circ$ , the clearance area between the ball and the seat of the hole is increased. ( $A_{c1} = \pi d^2(1 - \cos \alpha)/4 \cos \alpha$ ). Consequently, the amount of leakage is large enough to prevent the creation of the vacuum and the ball, in this case, will stay at the central region of the ball-housing. On the other hand, when the cone angle  $\beta$  is equal to or larger than  $150^\circ$ , the bottom of the inside casing is flat enough to produce instability in ball operation and the ball, in this case, will act in a random manner until it closes and remains on one of the two discharge tubes. These limitations have been verified experimentally and the operation

of the oscillator outside the above mentioned region has been found to be unstable. Table 5 gives the clearance area value for different cone angles.

Cone Angle $\theta$	150°	140°	130°	120°	110°
Clearance Area $A_c$	.03528A	.06418A	.10338A	.1547A	.22077A

← Range of Operation →  $A = \pi d^2/4$

TABLE 5

#### 2.5.5 Force Analysis Approach

This section deals with the investigation of the forces inside the ball-housing for the purpose of introducing the mathematical model for calculating the time  $t_2$ . In this study, it has been assumed that the ball is already outside the seat of the hole and starting to move to the other discharge hole. The possible forces acting on the ball are as follows:

1. The gravity force  $F_1$  or  $F_g$ .
2. The flow force  $F_2$  or  $F_f$ .
3. The suction force  $F_3$  or  $F_s$ .
4. The buoyant force  $F_4$  or  $F_B$ .

The direction of the gravity force is vertically downward and the direction of the buoyant force is vertically upward. The directions of the flow force and the suction force may be assumed towards the center of the opposite discharge hole as shown in

Figure 21.

For practical purposes, the time  $t_2$  remains approximately the same for both cases, oscillation with leakage and oscillation without leakage. The following represents the procedure to calculate the above forces ( $F_1, F_2, F_3, F_4$ ).

1.  $F_1 = m \times g = \text{gravity force } F_g$ ; where

$m$  = the mass of the ball.

$g$  = the gravitational acceleration.

2.  $F_2 = P_1 \times A_b = \text{flow force } F_f$ ; where

$P_1$  = mean value of the pressure inside the ball-housing.

$A_b$  = cross-section area of the ball-housing =  $\pi D^2/4$ .

$D$  = inside diameter of the ball-housing.

3.  $F_3 = \text{suction force } F_s$

= head loss due to sudden contraction  $\times$  specific weight of supply water  $\times$  cross-section area of the discharge tube.

=  $(\frac{K}{2g} V^2)(W_w)(\pi d^2/4)$ ; where

$V$  = discharge velocity.

$W_w$  = specific weight of supply water.

$d$  = discharge tube diameter.

$g$  = gravitational acceleration.

$K$  is a constant to be determined from Figure 22 according to the equation  $K = (\frac{1}{C_c} - 1)^2$  and  $C_c$  is the contraction

coefficient.

4.  $F_4 = V_b \times W_w = \text{buoyant force } F_B$ ; where  
 $V_b = \text{volume of the ball.}$   
 $W_w = \text{specific weight of the supply water.}$

Therefore,

$\Sigma F_{II}$  = Force summation in direction II (perpendicular to the inner ball-housing surface).

$$N_r - (F_1 - F_B) \cos a - (F_2 + F_3) \sin b = \text{mass} \times (a_G)_{II} = 0$$

$$N_r = (F_1 - F_B) \cos a + (F_2 + F_3) \sin b \quad (17)$$

where  $N_r$  = the normal force

$(a_G)_{II}$  = the ball acceleration in direction II

$\Sigma F_I$  = Force summation in direction I (parallel to the inner ball-housing surface)

$$(F_1 - F_B) \sin a + (F_2 + F_3) \cos b - F_r = \text{mass} \times (a_G)_I \quad (18)$$

where  $F_r$  = friction force between the ball and inner surface of the ball-housing.

$(a_G)_I$  = the ball acceleration in direction I.

$\Sigma M_G$  = moment balance around point G

$$F_r \cdot r = I_G \cdot \alpha \quad ; \text{ where} \quad (19)$$

$I_G$  = moment of inertia of the ball =  $\frac{2}{5} m \cdot r^2$

$r$  = ball radius

$\alpha$  = angular acceleration of the ball.

From Equation (19), it follows

$$F_r \cdot r = \frac{2}{5} m r^2 \cdot \alpha ; F_r = \frac{2}{5} m r \cdot \alpha \quad (20)$$

The maximum force which can be developed to prevent slipping is:

$$F_{\max} = \mu \cdot N_r = \mu [(F_1 - F_B) \cos a + (F_2 + F_3) \sin b], \text{ where}$$

$\mu$  = the coefficient of friction between the ball and the inner surface of the ball-housing.

If  $F_r > F_{\max}$ , the ball is rolling and slipping at the same time.

If  $F_r \leq F_{\max}$ , the ball is rolling without slipping.

It is assumed here that the ball is rolling without slipping. Thus,

$$\text{in this case [20]} \quad (a_G)_I = \alpha \cdot r \quad (21)$$

Substituting Equations (20) and (21), in Equation (18),

$$(F_1 - F_B) \sin a + (F_2 + F_3) \cos b - \frac{2}{5} m \cdot r \cdot \alpha = m \cdot \alpha \cdot r$$

$$(F_1 - F_B) \sin a + (F_2 + F_3) \cos b = 1.4 m \cdot r \cdot \alpha \quad (22)$$

From the equation for the distance travelled

$$Y = V_{in} \cdot t + \frac{1}{2} (a_G)_x \cdot t^2 ; \text{ where}$$

$V_{in}$  = initial velocity of the ball = 0.

$t$  = time.

$Y$  = distance travelled.

we obtain

$$Y = \frac{1}{2} (r \cdot \alpha) t^2 ; \alpha = 2Y / r t^2 \quad (23)$$

From Equations (22) and (23),

$$(F_1 - F_B) \sin a + (F_2 + F_3) \cos b = 1.4 m \cdot r \cdot \frac{2Y}{r t^2} = \frac{2.8m}{t^2} \left( \frac{Y - r \sin a}{\cos a} \right)$$

$$t^2 = \frac{2.8m(y-r\sin a)}{(F_1-F_B)\sin a \cos a + (F_2+F_3)\cos b \cos a}$$

$$t = \sqrt{\frac{2.8m(y-r\sin a)}{(F_1-F_B)\sin a \cos a + (F_2+F_3)\cos b \cos a}}$$

Since the total travelling distance is  $2Y$ , the time  $t_2$  may be assumed to be equal to  $2t$ .

$$t_2 = 2 \sqrt{\frac{2.8m(y-r\sin a)}{(mg - \frac{4}{3}\pi r^3 W_W)\sin a \cos a + (\frac{P_1 \pi D^2}{4} + \frac{.3693\pi W_W V^2 d^2}{8g})\cos b \cos a}} \quad (24)$$

or

$$t_2 = 3.346 \sqrt{\frac{m(y-r\sin a)/\cos a}{(mg - 4.18r^3 W_W)\sin a + (.78P_1 D^2 + .0045W_W V^2 d^2)\cos b}}$$

and the range of validity of this equation is  $15^\circ < \alpha < 35^\circ$  or  $110^\circ < \epsilon < 150^\circ$ .

Table 6 gives the angles  $b$  for different cone angles.

Cone Angle $\epsilon$	$150^\circ$	$140^\circ$	$130^\circ$	$120^\circ$	$110^\circ$
Angle $b$	$20.50^\circ$	$16.25^\circ$	$12.25^\circ$	$9.00^\circ$	$3.50^\circ$

Range of Validity

TABLE 6

Equation (24) has been solved using a FORTRAN program (see Appendix B). Figures 23, 24 and 25 illustrate the experimental and theoretical results for the time  $t_2$  for different angles  $\delta$  of  $30^\circ$ ,  $25^\circ$  and  $20^\circ$  respectively. The theoretical results show good agreement with the experimental results. From Figures 23, 24 and 25, it is concluded that the angle of inclination  $\delta$  of the inner ball-housing has negligible effect on time  $t_2$ . The main factors affecting time  $t_2$  are the discharge tube length and the initial discharge velocity.

As mentioned before in Section 2.3 of this Chapter, the total time  $T$  is the time necessary for one complete cycle.  $T$  is equal to  $2(t_1 + t_2)$  millisec/cycle which corresponds to a frequency of  $0.5(t_1 + t_2)^{-1}$  Hertz. Figures 26, 27, 28 and 29 represent the experimental and theoretical results giving the frequency for different tube lengths and different angles of  $\delta$ ,  $30^\circ$ ,  $25^\circ$ ,  $20^\circ$ , for the case without leakage.

## CHAPTER 3

## EXPERIMENTAL INVESTIGATION

3.1 INTRODUCTION

In order to verify the theoretical work developed for the ball oscillator, experimental work was carried out using a prototype oscillator of flexible design. An assembly drawing of the prototype with its components is shown in Figure 30. Provision is made in the prototype for design flexibility in three main directions:

1. For attaching discharge tubes of different lengths.
2. For inserting ball-housings with different angles of inclination.
3. For inserting a specially designed ball-housing for the case without leakage.

The experimental work carried out in the Fluid Control Center laboratories fulfilled three distinct purposes:

1. First, to obtain qualitative information on the range of the frequency of oscillation for different tube lengths and different discharge velocities for both cases, with and without leakage.
2. Secondly, to experimentally verify the theoretical results obtained by solving the developed differential equation



governing the fluid slug motion during the time  $t_1$ .

3. Finally, to check the validity of the developed mathematical model used to calculate the time  $t_2$ .

### 3.2 COMPONENTS OF THE PROTOTYPE OSCILLATOR

The components of the prototype oscillator consist of the following:

1. The main outside body of the prototype, Figure 31.
2. Inside core with angle  $\alpha = 35^\circ$ , Figure 32, with leakage.
3. Inside core with angle  $\alpha = 30^\circ$ , Figure 33, with leakage.
4. Inside core with angle  $\alpha = 25^\circ$ , Figure 34, with leakage.
5. Inside core with angle  $\alpha = 20^\circ$ , Figure 35, with leakage.
6. Inside core with angle  $\alpha = 15^\circ$ , Figure 36, with leakage.
7. Specially designed ball-housing for the case without leakage, Figure 37.

The case of no-leakage is achieved by the specially designed ball-housing in which the inside housing has a V-shape and the discharge holes are drilled perpendicularly on the housing surface. Also, in order to improve the no-leakage case, two rubber rings may be attached at the inlet of the discharge tubes.

8. Locking nut, Figure 38.
9. Twin sets of different tube lengths in order to obtain different discharge tube lengths, 3, 4.5, 6, 9, 12, 18, 24 inches, Figure 39.

10. Rubber gaskets to prevent leakage between the different parts during operation.
11. Balls of different materials with a diameter of  $5/8$  inch. Two balls were used during the experimental work, a rubber ball of specific weight  $108 \text{ lb/ft}^3$ , and a steel ball of specific weight  $485 \text{ lb/ft}^3$ .
12. A long connecting tube between the supply pressure and the prototype (approximately 56 inches long).

The material used in the construction of all the previous components of the prototype is plexi-glass, except for the ball and the locking nut which is in brass. The machining of all the components was carried out in the Machine Shop of Sir George Williams Campus. One of the best advantages of plexi-glass is its transparency which permits the viewing of the inside of the prototype, during operation to observe ball motion and to verify the forward and reverse motion of the fluid slug by taking motion pictures using a high speed camera.

### 3.3 VERIFICATION OF THE SLUG MOTION AND BALL OSCILLATIONS

The first step in the experimental work in the laboratory was to check two main concepts:

1. The predicted behaviour of the slug motion when the ball-valve closes the upstream end of the discharge tube.
2. The ball motion inside the casing to determine whether the ball always moves in contact with the lower surface of the inner casing or whether it jumps in the liquid from one

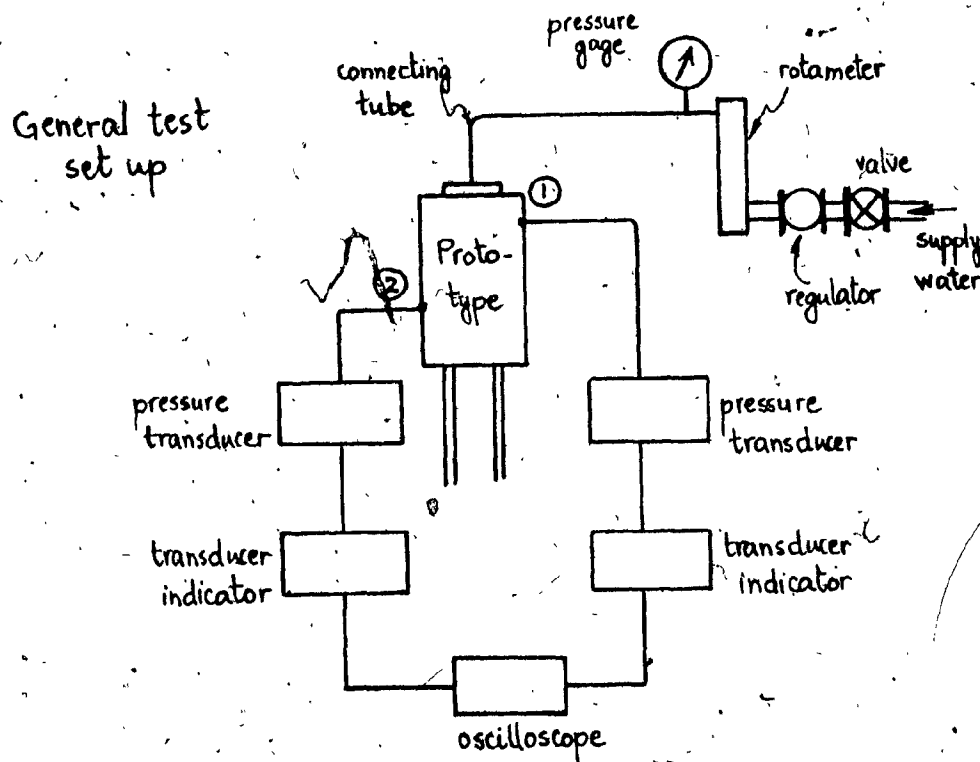
hole to the other.

In order to achieve confidence over the theoretical concept of the oscillator operation, three different motion films have been taken using a high speed camera with a speed of 4000 frames per second. The first film concentrates on the lower part of the prototype to show clearly the forward and reverse slug motion. The second film shows the upper part of the prototype to demonstrate the slug motion and the ball motion during operation. Finally, the third film shows the entire prototype during operation. The behaviour of the slug motion and ball motion shown in the three films correlates well with the theoretical predictions.

### 3.4 EXPERIMENTAL APPARATUS

The general set-up of the experimental apparatus is shown in the following figure. It consists of the fluid oscillator prototype with all its components connected to the supply line and to the measurement unit. The measurement unit consists of two pressure transducers with their associated indicators, a storage oscilloscope and an oscilloscope camera. The water supply to the fluid oscillator is obtained from the water main through a regulator and a long connecting tube.

All measurements are taken at points 1 and 2 as shown in the assembly drawing, Figure 30. Since the measurements are made with a pressure transducer, the question of frequency response of the transducer arises. The situation wherein a liquid is being used in a



transducer is entirely different from that of a gas filled apparatus. A liquid is characterized by a high density and stiffness, while a gas at ordinary pressure has a density and stiffness several orders lower in magnitude than those of a liquid. This causes the transducer, which is comprised of a mass-spring system, to change its natural frequency as soon as it is charged with the liquid [21]. This indicates that the length of tubing, connecting the prototype and the transducers at points 1 and 2, has an effect on the natural frequency of the transducers, thereby affecting the oscillator frequency measurement. Hence it is desirable to minimize the length of the interconnecting tubing between oscillator and transducers.

### 3.5 PROCEDURE

The first step in the experiments is the calibration of the pressure transducers. A suitable sensitivity of the transducer is selected and a known supply pressure level is applied. The transducer indicator is adjusted to the required reading. Now the supply pressure is cut off and the indicator is checked for zero reading. If it does not read zero, it is adjusted to do so. The process is repeated until zero reading is obtained with zero input and full-scale reading with the full input. The calibration of the transducer is then complete.

A specific supply pressure is now applied to the prototype. The flow rate is measured directly from the rotameter and the corresponding discharge velocity in ft/sec is calculated as follows:

flow rate =  $2 \times A \times V$ , where

A = cross-section area of the discharge tube.

V = discharge velocity prior to closure.

Figure 40 represents the relationship, obtained experimentally, between the supply pressure and the rotameter reading. Figure 41 illustrates the relationship between the supply pressure and the calculated discharge velocity (ft/sec). At any particular discharge velocity, the pressure distribution at points 1 and 2, during the ball oscillation, is displayed on the oscilloscope screen. The above experimental procedure is repeated many times for different supply pressures (10 to about 65 psig which corresponds to discharge velocities of 7 to 22 ft/sec) and for various tube lengths (3, 4.5,

6, 9, 12, 18 and 24 inches). The experimental results for time  $t_1$  and time  $t_2$  are obtained directly from the oscilloscope traces. A typical pressure distribution is shown in Figure 42 for points 1 and 2. Figures 43 to 50 represent some oscilloscope trace photographs for typical pressure distributions at points 1 and 2 for various supply pressures and tube lengths.

## CHAPTER 4

## DISCUSSION OF THE RESULTS

4.1 INTRODUCTION

The theoretical analysis developed for the ball oscillator has been divided into two different parts. The first part deals with the forward and reverse motions of the fluid slug, during the period ( $t_1$ ) when the ball remains seated on the upstream end of the discharge tube. For this part a differential equation governing the fluid slug motion is derived and solved by a MIMIC program. In the second part of the analysis, a mathematical lumped-parameter model is developed in order to calculate the time ( $t_2$ ) necessary for the ball to move from one hole to the other. This mathematical model has been solved by a FORTRAN program (see Appendix A for the MIMIC program and Appendix B for the FORTRAN program).

The behaviour of the fluid slug motion and the oscillation of the ball during operation have been carefully observed and verified by means of three motion picture films taken using a high speed camera (4000 frames per second).

The theoretical results for the times  $t_1$  and  $t_2$  showed a good agreement with the corresponding experimental results. Consequently, the theoretically predicted oscillation closely agrees with the experimentally measured frequency.

The oscillation frequency depends on a number of parameters

such as the initial discharge velocity, tube length, design of the oscillator with leakage or without leakage, the angle of inclination  $\alpha$  of the inner casing and the specific weight of the ball (i.e. steel ball or rubber ball). The effects of these variables are discussed below.

#### 4.2 EFFECT OF INITIAL DISCHARGE VELOCITY

A change in the initial discharge velocity introduces a change in the oscillation frequency. The initial discharge velocity increases as the supply pressure increases. Figure 48 shows the relationship between the supply pressure and the initial discharge velocity. As the discharge velocity (or the supply pressure) increases, the frequency first increases up to a certain supply pressure range, which is dependent upon the tube length, and then starts to decrease. This supply pressure range becomes higher as the tube length is decreased.

#### 4.3 EFFECT OF TUBE LENGTH

The tube length appears to be the most important parameter affecting the frequency. First of all, it can be seen from Figures 25, 26 and 27 that for short tubes (approximately less than 3 inches) the ball may not be able to oscillate properly because the time  $t_1$  and the corresponding maximum slug displacement are relatively very small. This fact has been confirmed experimentally by using an oscillator prototype with short tube length and observing that the



ball had ceased to oscillate. Generally speaking, as the length of the tube decreases, the ball frequency increases, especially for high discharge velocities. For relatively small discharge velocities, the frequency increases as the length of the tube increases. Usually, the oscillator operation is in the first region where the supply pressure is high enough to maintain and to provide stable working oscillations.

#### 4.4 EFFECT OF OSCILLATOR DESIGN, WITH OR WITHOUT LEAKAGE

It is recommended that the design with leakage be used. As shown in Figure 37, the inner casing of the no-leakage oscillator is complicated and some accuracy is required during the machining process to drill the two discharge holes perpendicularly on the V-shape of the inner casing. Also, this design is composed of two separate parts glued together. On the other hand, for the case with leakage, the inner casing is simple in construction as it is composed of only a single part. Generally, the frequency obtained by the 'no-leakage' design is less than the frequency obtained by the 'leakage' design for the same tube length and supply pressure, as shown in Figures 33 to 36. This is due to the amount of leakage accumulated on the top of the fluid slug and the consequent decrease in time  $t_1$ .

#### 4.5 EFFECT OF THE ANGLE $\alpha$ OF THE INNER CASING

As explained in Section 2.4.4.2, the amount of leakage is increased as the angle  $\alpha$  increases. When  $\alpha$  is equal to  $90^\circ$ , the

amount of leakage tends towards infinity. The oscillator may not operate at all if the leakage is too much, because in this case, the vacuum may not occur. As angle  $\alpha$  decreases, the leakage decreases and time  $t_1$  increases and consequently the ball frequency decreases. As a matter of fact, the ball may not operate if the angle  $\alpha$  is too small (less than  $20^\circ$ ) because in this case, the bottom of the inner casing is flat enough to create instability in ball motion. Figures 33, 34 and 35 represent the results for the frequency for different angles  $\alpha$  of  $30^\circ$ ,  $25^\circ$  and  $20^\circ$  respectively. As mentioned in Chapter 2, the range of operation found experimentally is  $15^\circ < \alpha < 35^\circ$ .

#### 4.6 EFFECT OF THE BALL MATERIAL

During the experimental work, two types of balls have been used, each of 5/8 inch diameter. The size of the ball should be suitable for the inner casing geometry. The first one is a rubber ball of specific weight  $108 \text{ lb/ft}^3$  and the second ball is a steel one of specific weight  $485 \text{ lb/ft}^3$ . The time  $t_1$  is the same for both balls since the clearance area does not vary with the ball material. The time  $t_2$ , however, is dependent upon the ball material. It has been found experimentally and theoretically that the time  $t_2$  for a steel ball is approximately twice that for a rubber ball of the same diameter.

Due to the variation in time  $t_2$ , the frequency obtained with the steel ball is approximately 75% of that obtained with the rubber ball. Also, the heavier steel ball requires a higher supply pressure.

for both the start as well as to sustain oscillations. Thus, the oscillator using the rubber ball is preferred.

## CHAPTER 5

## CONCLUSIONS AND RECOMMENDATIONS FOR FUTURE WORK

5.1 CONCLUSIONS

A theoretical analysis of the ball oscillator is presented.

This analysis is divided into two parts. The first part predicts the time necessary for the forward and reverse motions of the fluid slug and the solution of the formulated differential equation is carried out by a MIMIC program. The second part predicts the time required for the ball to move from one discharge hole to the other, and the solution of the formulated mathematical model (lumped parameter type) is carried out by a FORTRAN program. The theoretical results are in good agreement with the experimental results in predicting the ball frequency.

Based on the theoretical and experimental work, it can be concluded that the parameters which effect the oscillation frequency are the initial discharge velocity which is directly related to the supply pressure, the length of the discharge tube, the design of the oscillator with leakage or without leakage, the angle  $\delta$  of the inner casing inclination and the specific weight of the ball. The length of the discharge tube and the initial discharge velocity are the most important variables affecting the frequency.

The following remarks on the oscillator are considered to be significant:

1. The oscillator may not be able to operate with very short tubes (less than 3 inches).
2. It is recommended to use an oscillator design with leakage due to simplicity in design and construction.
3. A rubber ball is better than a steel ball. A steel ball needs higher supply pressure for sustaining oscillations.
4. The amount of leakage should not be too high, otherwise the necessary vapor pressure will not exist.
5. The ball oscillator is self-starting except in the vertical position.

The theory developed could be used as a basis for designing a ball oscillator to give a certain range of frequencies. The theory can be applied in the design of oscillators for specific applications such as a car wash, cleaning devices with water and a pulsating showerhead.

## 5.2 RECOMMENDATIONS FOR FUTURE WORK

Some suggestions for future extensions of this work are outlined below:

1. The theoretical analysis may be done in only one part instead of in two different separate parts. The new analysis could end by studying the pressure distribution inside the inner casing and the pressure distribution under the ball seat. Detailed knowledge of these distributions could improve the prediction of the device behaviour.

2. A detailed study of the stability of the ball could be conducted. This would assist the solution of the problem of self-starting in the vertical position.

REFERENCES

1. Kwok, C.K. and Cheng, R., "A Liquid Operated Oscillator". Adv. in Instrum., Vol. 28, Annual ISA Conference, 28th, Proc., Houston, Texas, Oct. 15-18, 1973, Part 4, Paper 830.
2. Kwok, C.K., "A Fluid Oscillator and Its Applications". Proceedings of the 5th Cranfield Fluidics Conference, Uppsala, Sweden, June 1972.
3. Sankar, S., "Simulation of a Diaphragm Type Fluid Oscillator". M.Eng. Thesis at Sir George Williams University, Mechanical Engineering Department, Montreal, Canada, August 1971.
4. Mueller, G.S. and Sankar, S., "A Diaphragm Type Fluid Oscillator: Analysis and Simulation". Fluidics Quarterly, Vol. 6, No. 1, January 1974.
5. Curry, W.A., "Sprinkler Control Means and Combination". U.S. Patent 3,321,138, May 1967.
6. King, H. and Brater, E., "Handbook of Hydraulics". McGraw-Hill Book Company, 1963, pp. 6-6/6-10.
7. Moody, L.F., "Friction Factors for Pipe Flow". Transactions of the American Society of Mechanical Engineers, Vol. 66, November 1944, pp. 671-678.
8. "Flow of Fluids Through Valves, Fittings and Pipe". by the Engineering Division, Technical Paper No. 410-C, Crane Co., Chicago, U.S.A.
9. Binder, R.C., "Fluid Mechanics". Prentice-Hall Book Company, New Jersey, 1962, pp. 44-46, 110-112.
10. Streeter, V.L. and Wylie, E.B., "Fluid Mechanics". McGraw-Hill Book Company, sixth edition, 1975, pp. 113-114, 116, 146, 292-300, 305.
11. Dally, James W. and Harleman, Donald R.F., "Fluid Dynamics". Addison-Wesley Publishing Company Inc., 1973, pp. 264, 270-275, 76-84.
12. Schlichting, H., "Boundary Layer Theory". McGraw-Hill Book Company, New York, sixth edition, 1968, pp. 560-563.

13. Li, Wen-Hsiung, "Mechanics of Pipe Flow Following Column Separation".  
Journal of the Engineering Mechanics Division, Proceedings of the American Society of Civil Engineers, ASCE, Vol. 88, No. EM4, August 1962, pp. 97-118.
14. Rohsenow, W.M. and Choi, H.Y., "Heat, Mass and Momentum Transfer".  
Prentice-Hall Book Company, New Jersey, 1961, pp. 56-60.
15. Safwat, H.H., "Water Column Separation and Cavitation in Short Pipelines".  
ASME Paper 75-FE-33, May 1975.
16. Swaffield, J.A., "A Study of the Influence of Air Release on Column Separation in an Aviation Kerosine Pipeline".  
Proceedings of the Institution of Mechanical Engineers, Vol. 186, pp. 693-703.
17. De Bernardinis, B.G. Federici and Siccardi, F., "Transient with Liquid Column Separation: Numerical Evaluation and Comparison with Experimental Results".  
L'Energia Elettrica, N-9, pp. 471-477.
18. Katz, S. and Chai, D., "Column Separation as a Feedback Mechanism in Liquid Oscillators".  
Paper under publication in the ASME, January 1977.
19. Hughes, F.W. and Brighton, J.A., "Fluid Dynamics".  
Schaums outline series - McGraw-Hill Book Company, Chapter 3 - Mathematical Models of Fluid Control, p. 26.
20. Higdon, A. and Stiles, W., "Engineering Mechanics". Chapter 10,  
Prentice-Hall Book Company, New Jersey, third edition.
21. White, Gifford, "Liquid Filled Pressure Gage Systems".  
Statham Instruments Note No. 7, Statham Instruments, Inc.,  
Los Angeles, California, U.S.A.



FIGURES

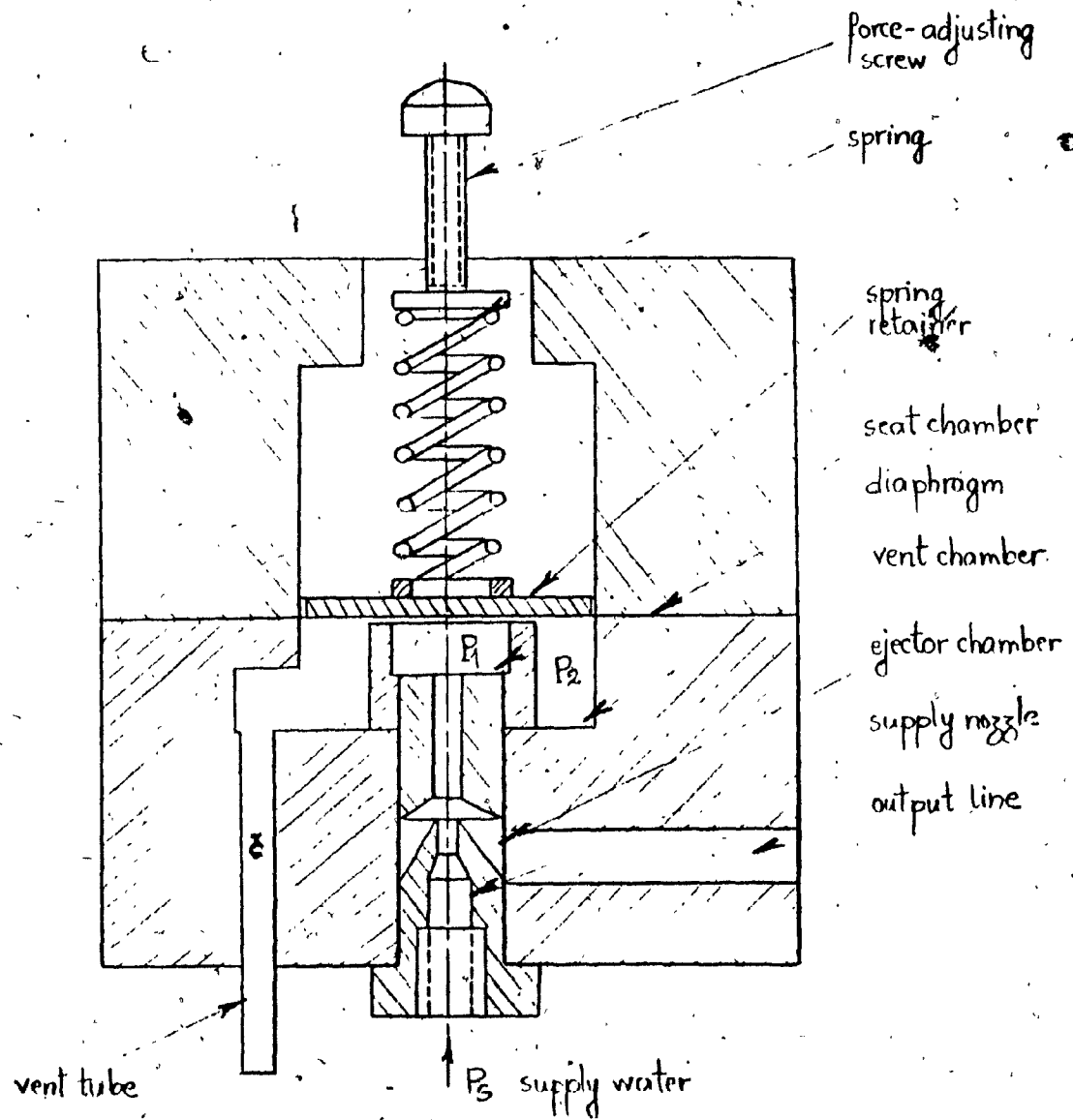


Figure 1. Cross sectional view of fluid oscillator.

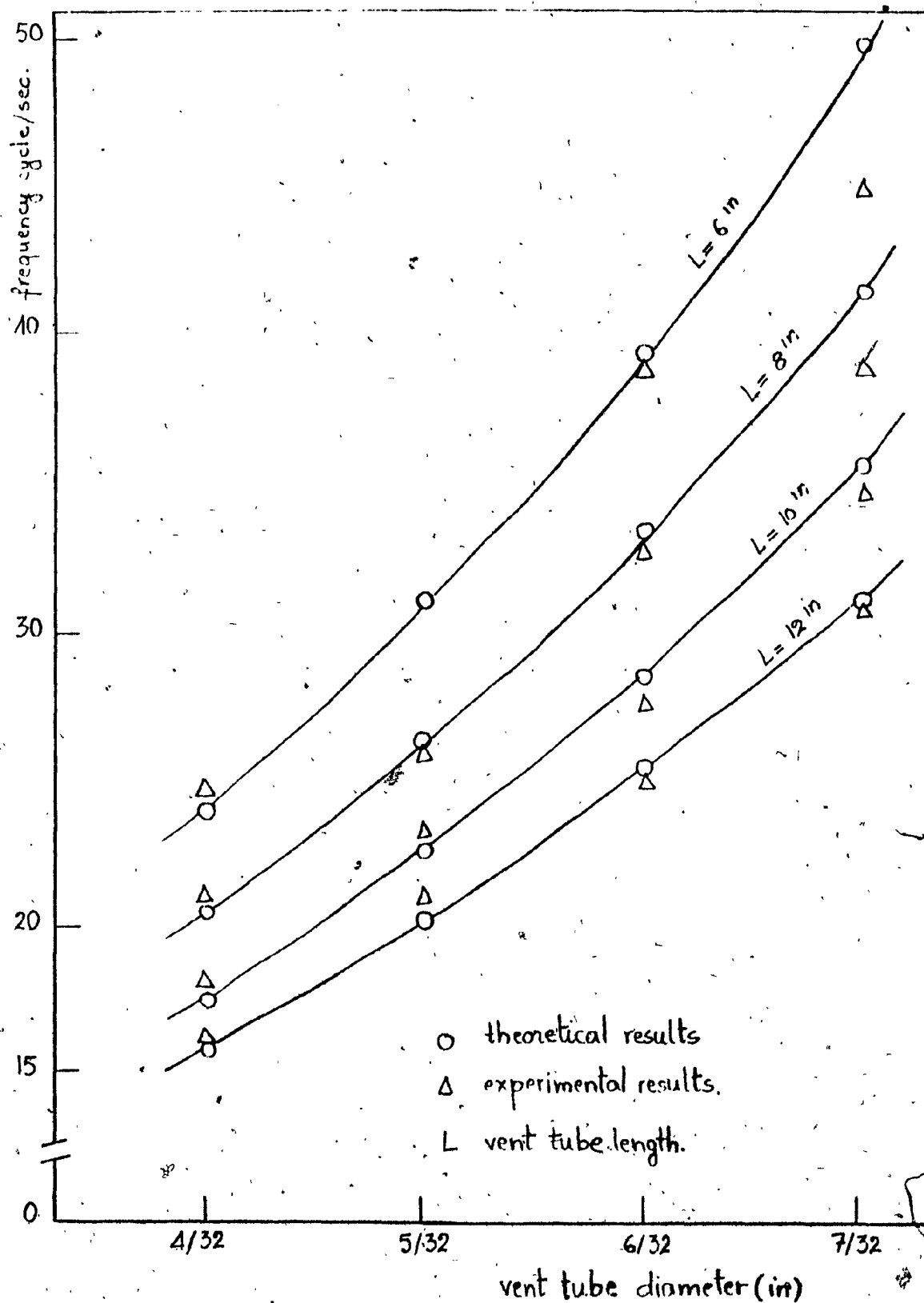


Figure 2 - effect of vent tube geometry on frequency.

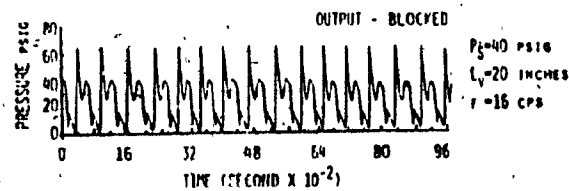
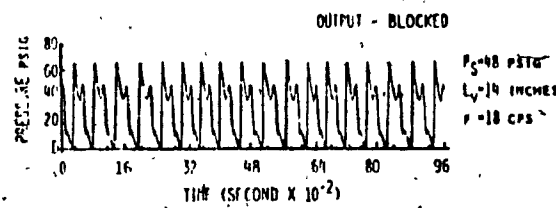
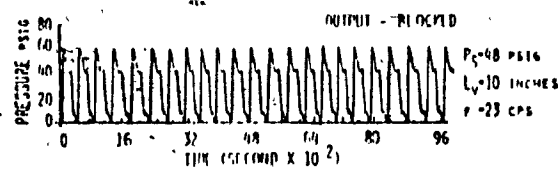


Figure 3 - Typical oscillator output pressure waveforms.

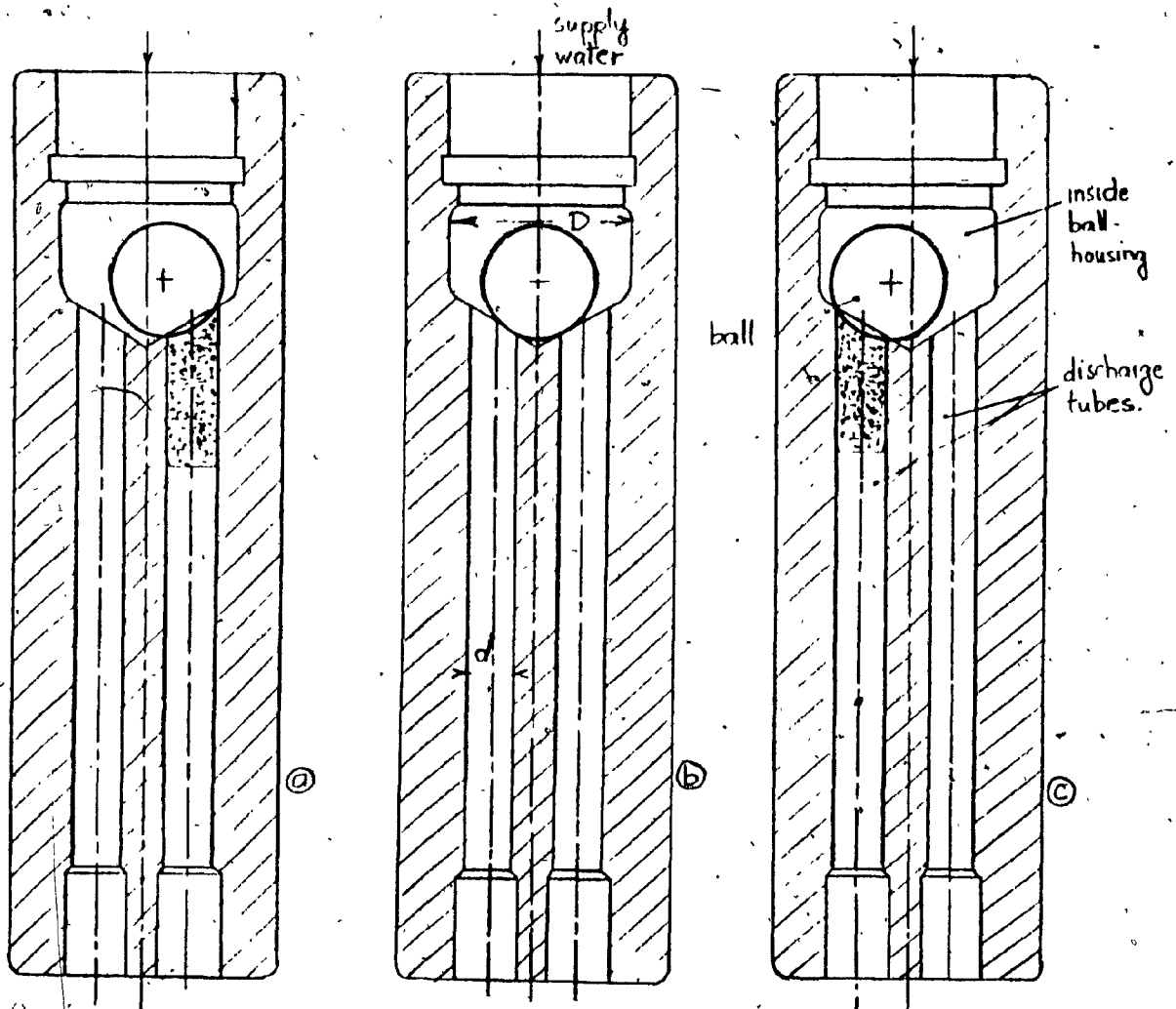


Figure 4 - General form of the ball-oscillator.

- a - ball closing right discharge tube
- b - ball moving to the left discharge tube.
- c - ball closing left discharge tube.

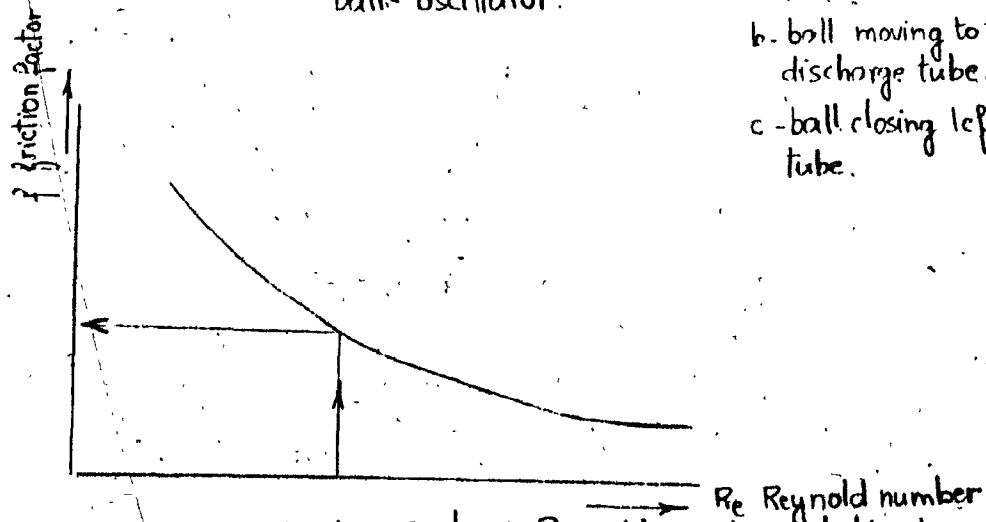


Figure 5 - friction factor & Reynold number relationship

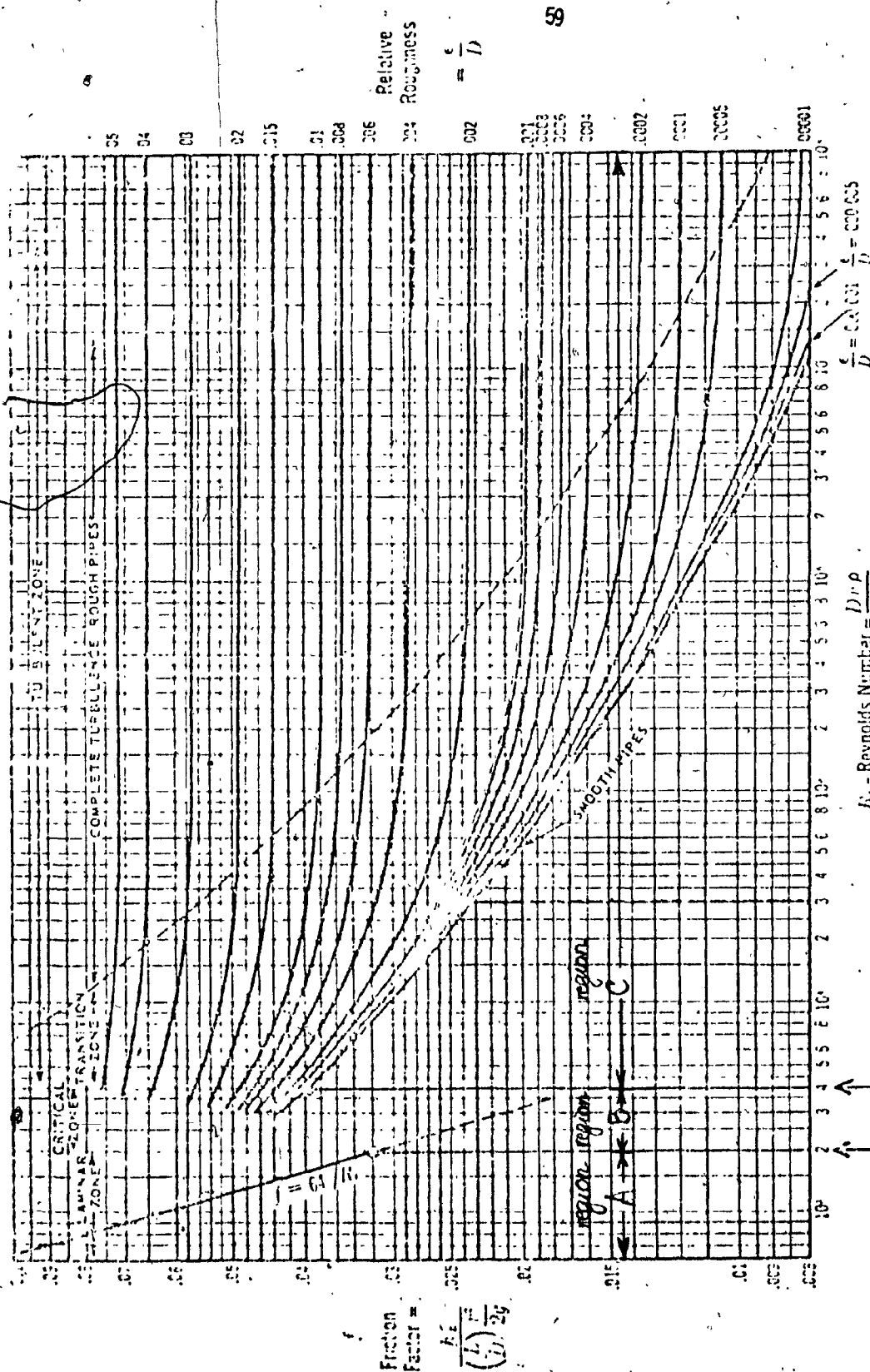


Figure 6- Moody Chart

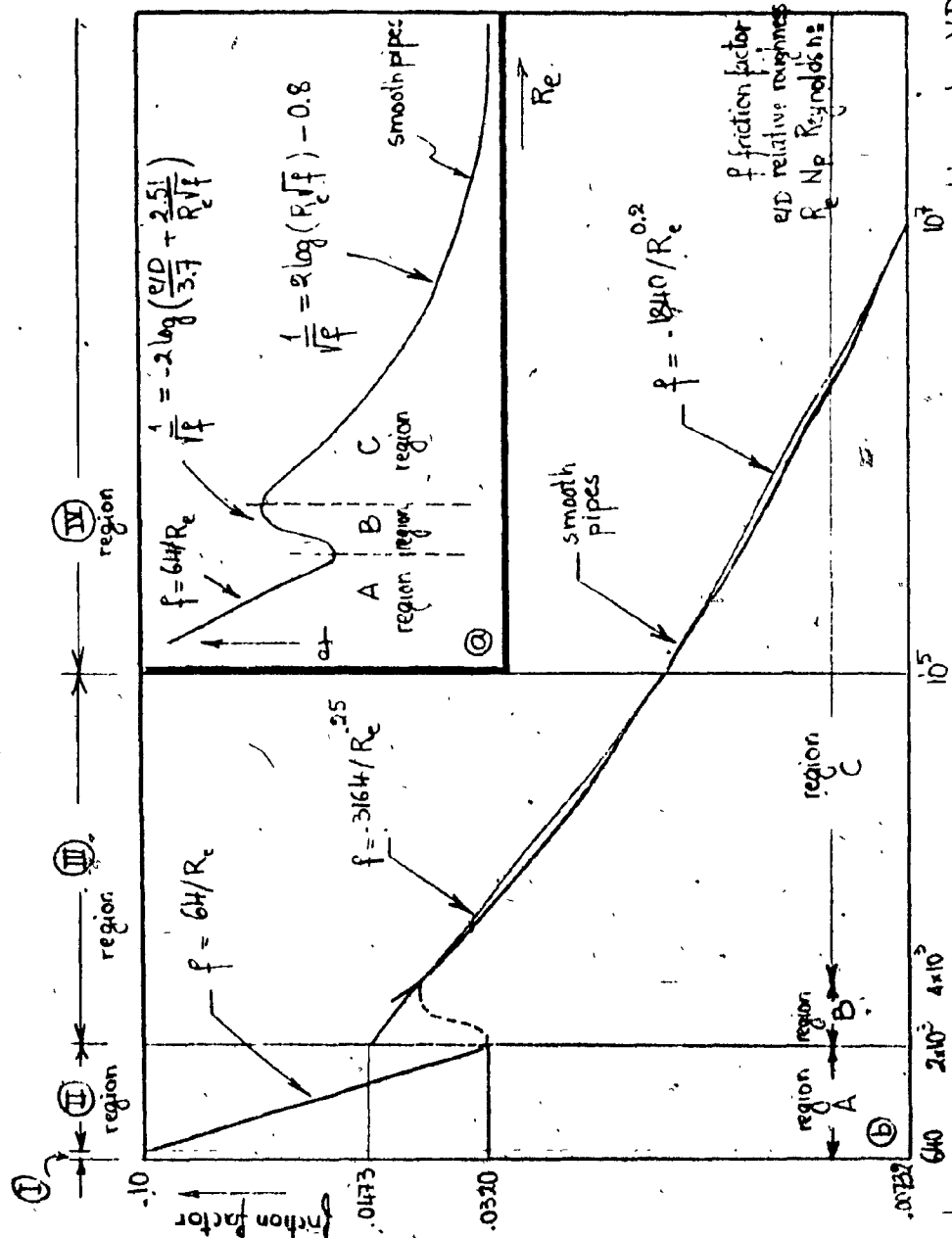


Figure 7 - Linear approximation of the smooth pipes curve.

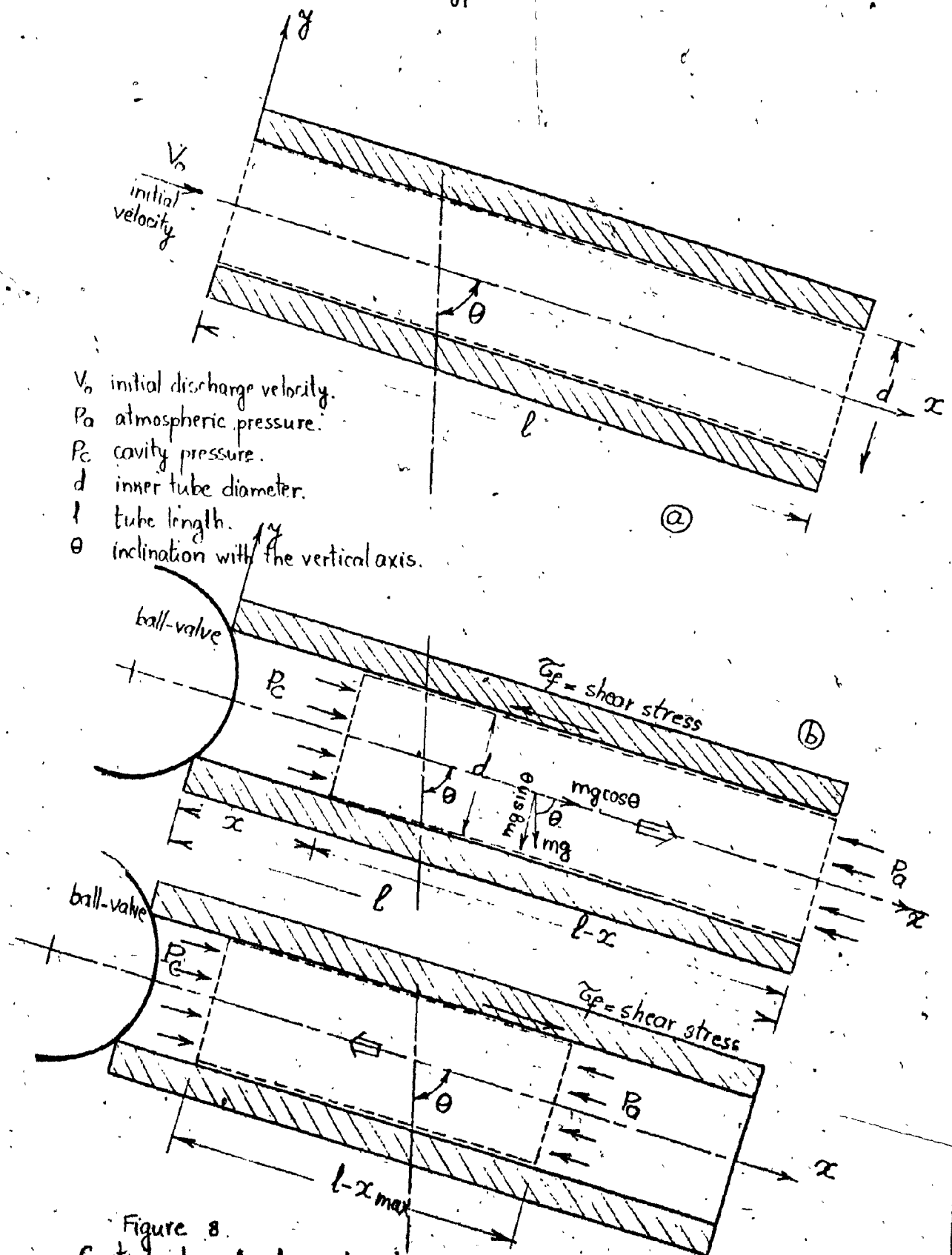


Figure 8.  
Control volume for forward and reverse slug motion (without leakage)



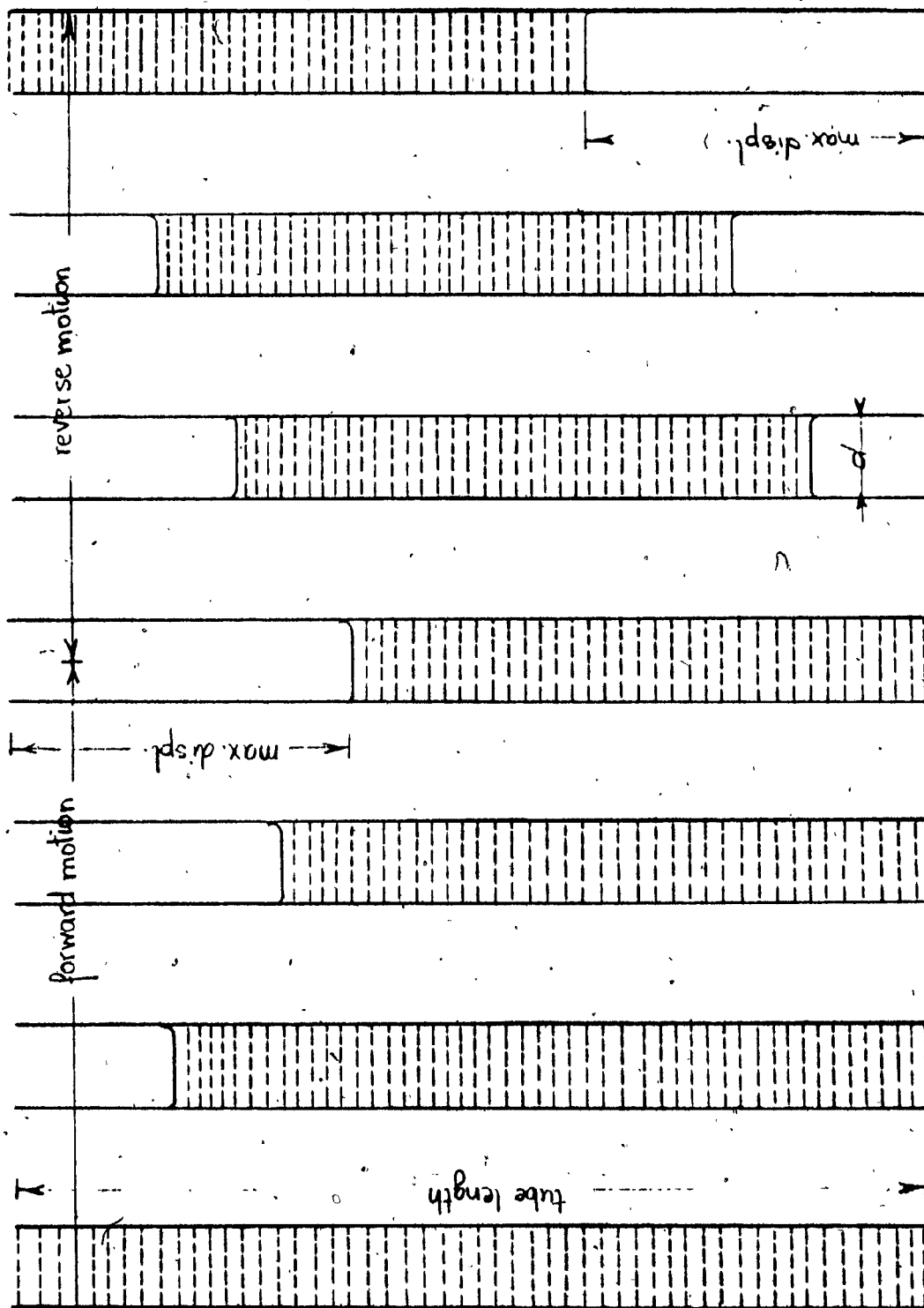
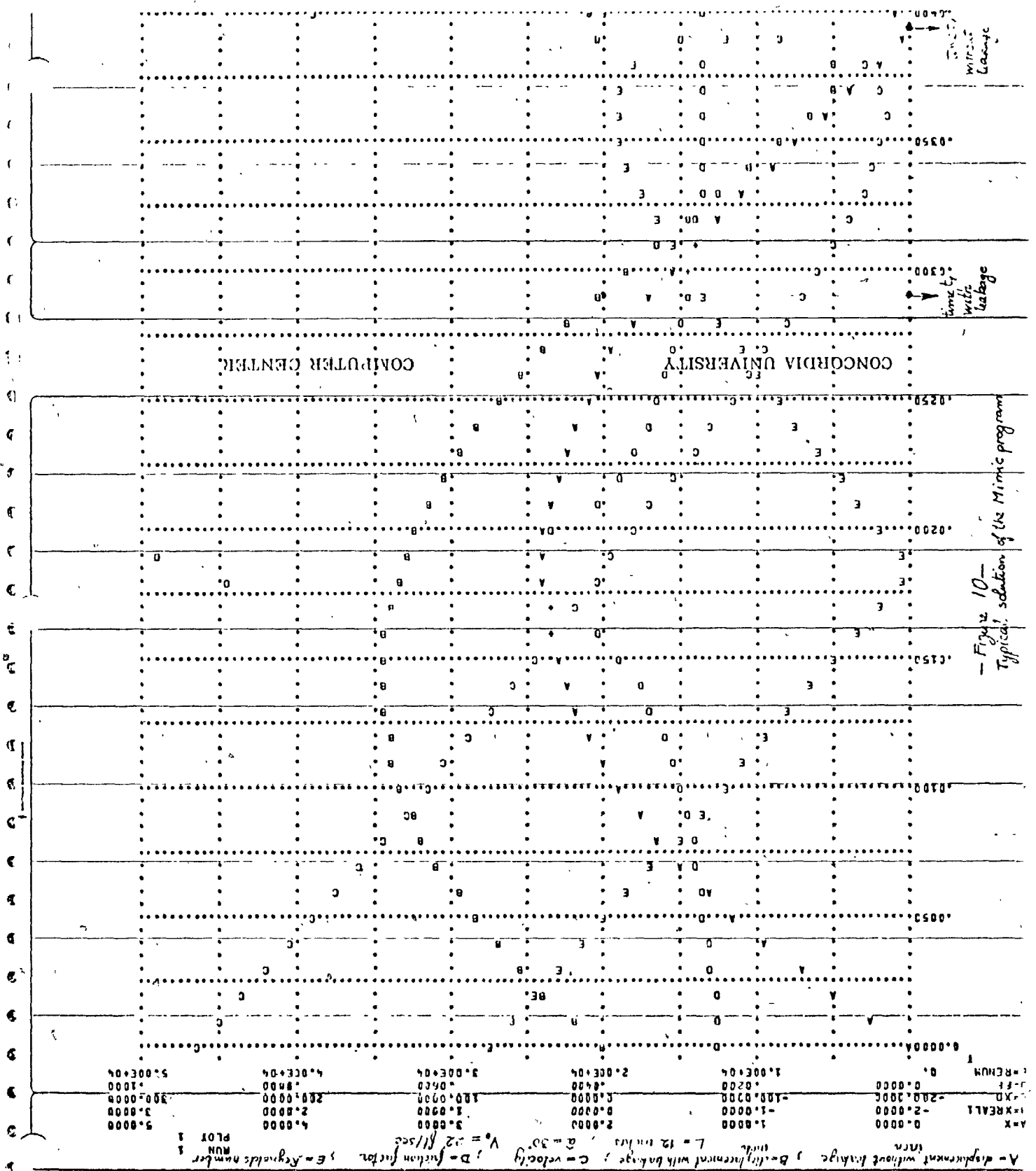
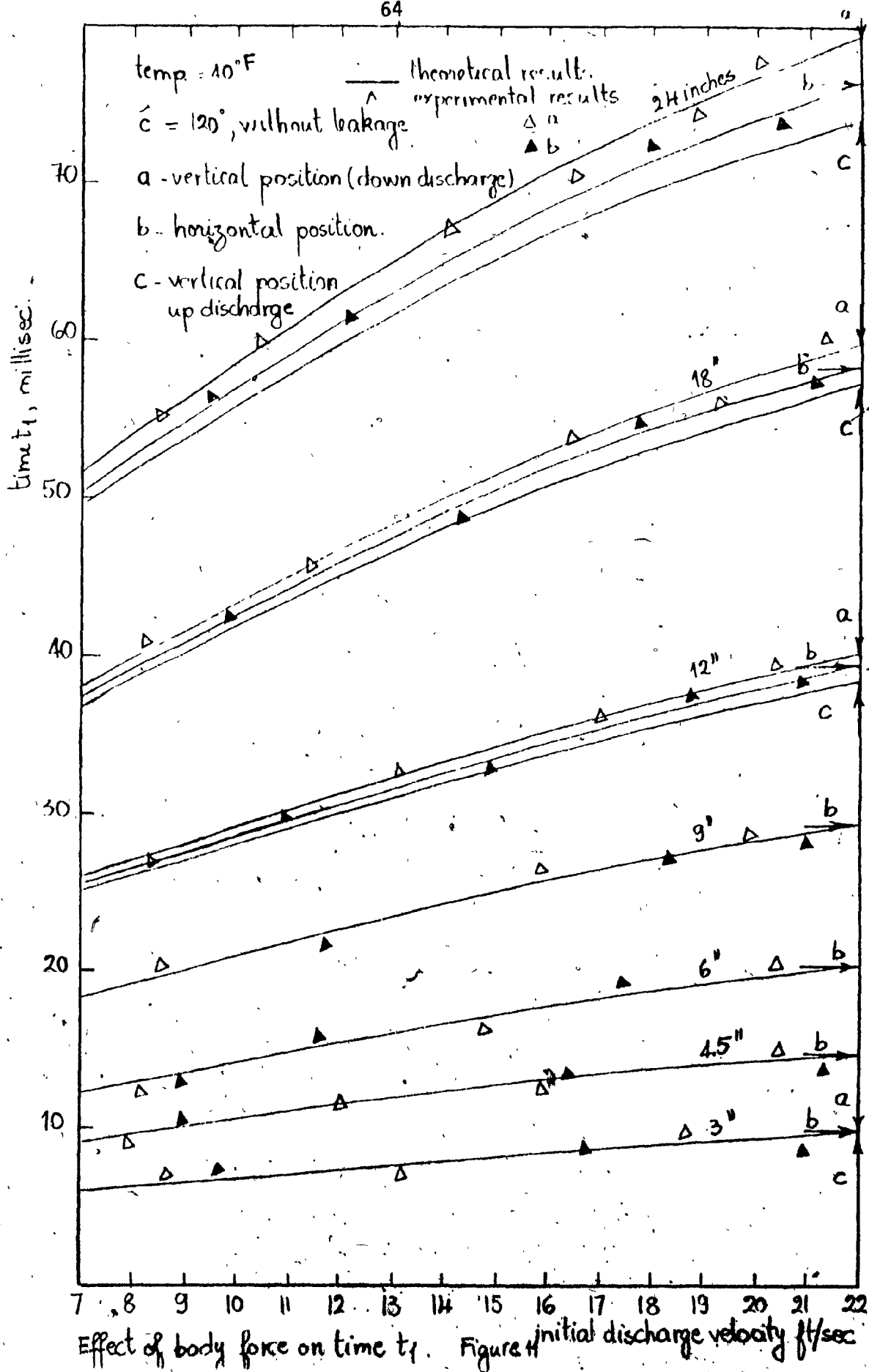
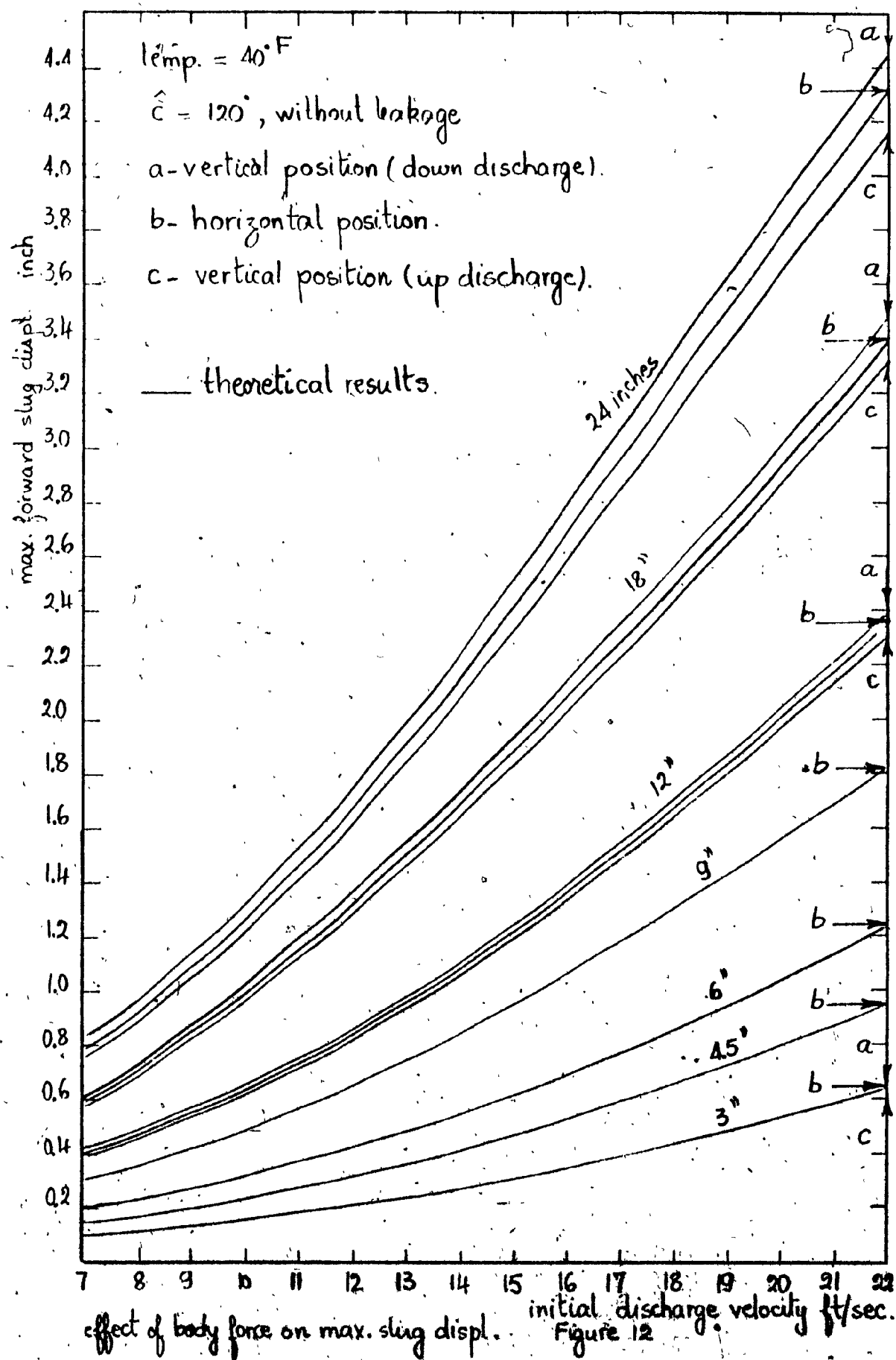


Figure 9 - Reverse and forward slug motion (without leakage)  
(not to scale)







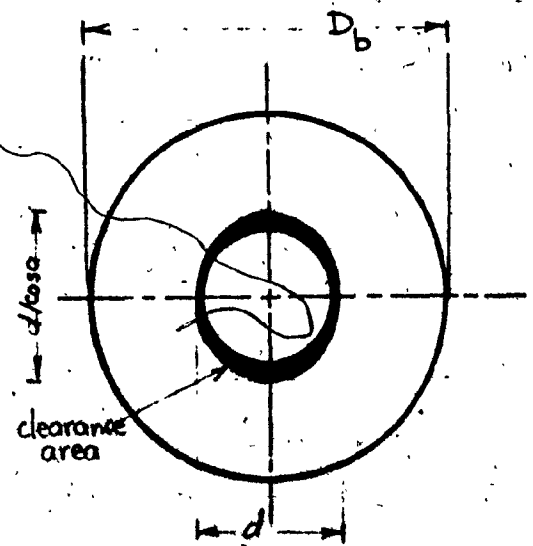
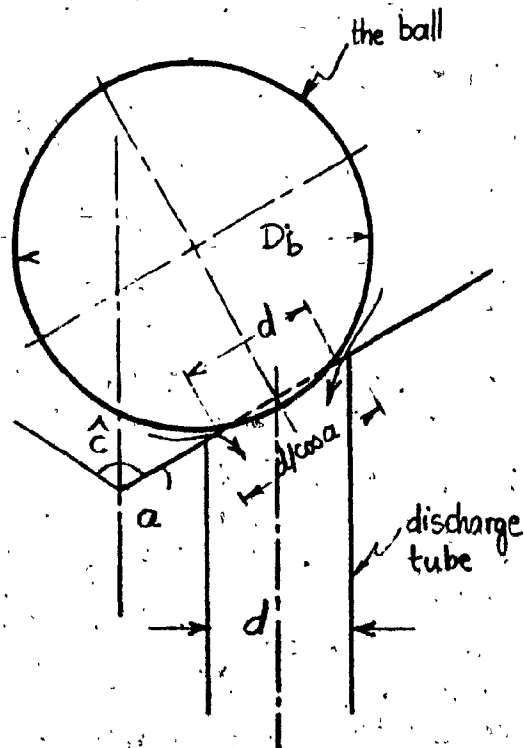
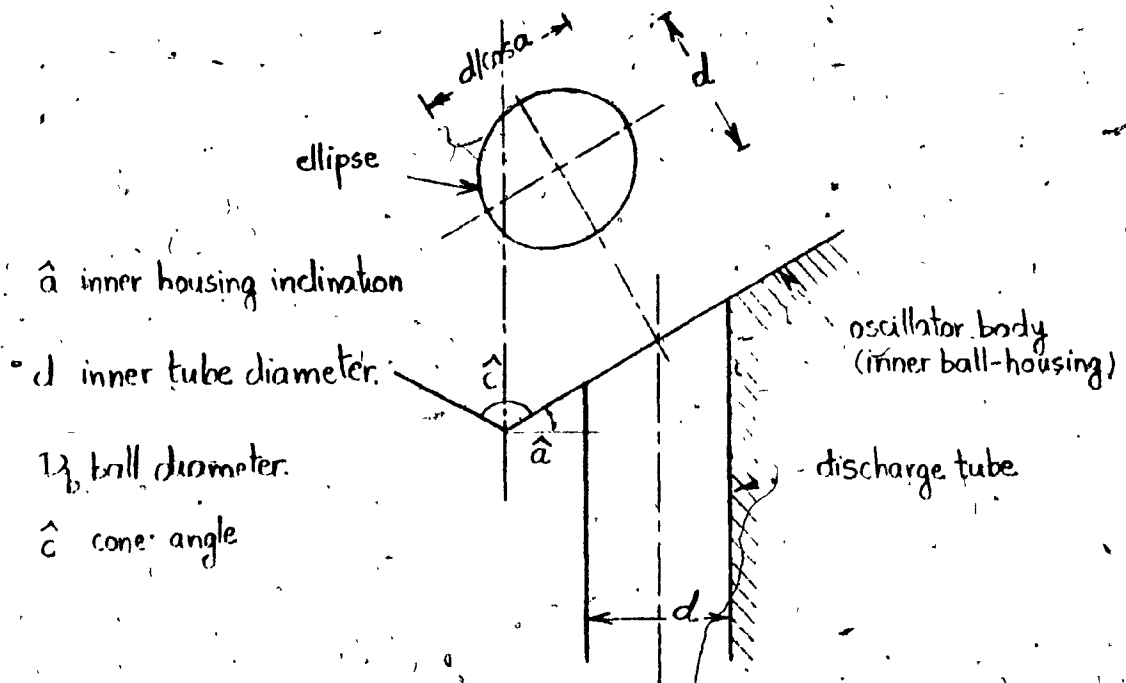


Figure 13 - Clearance Area

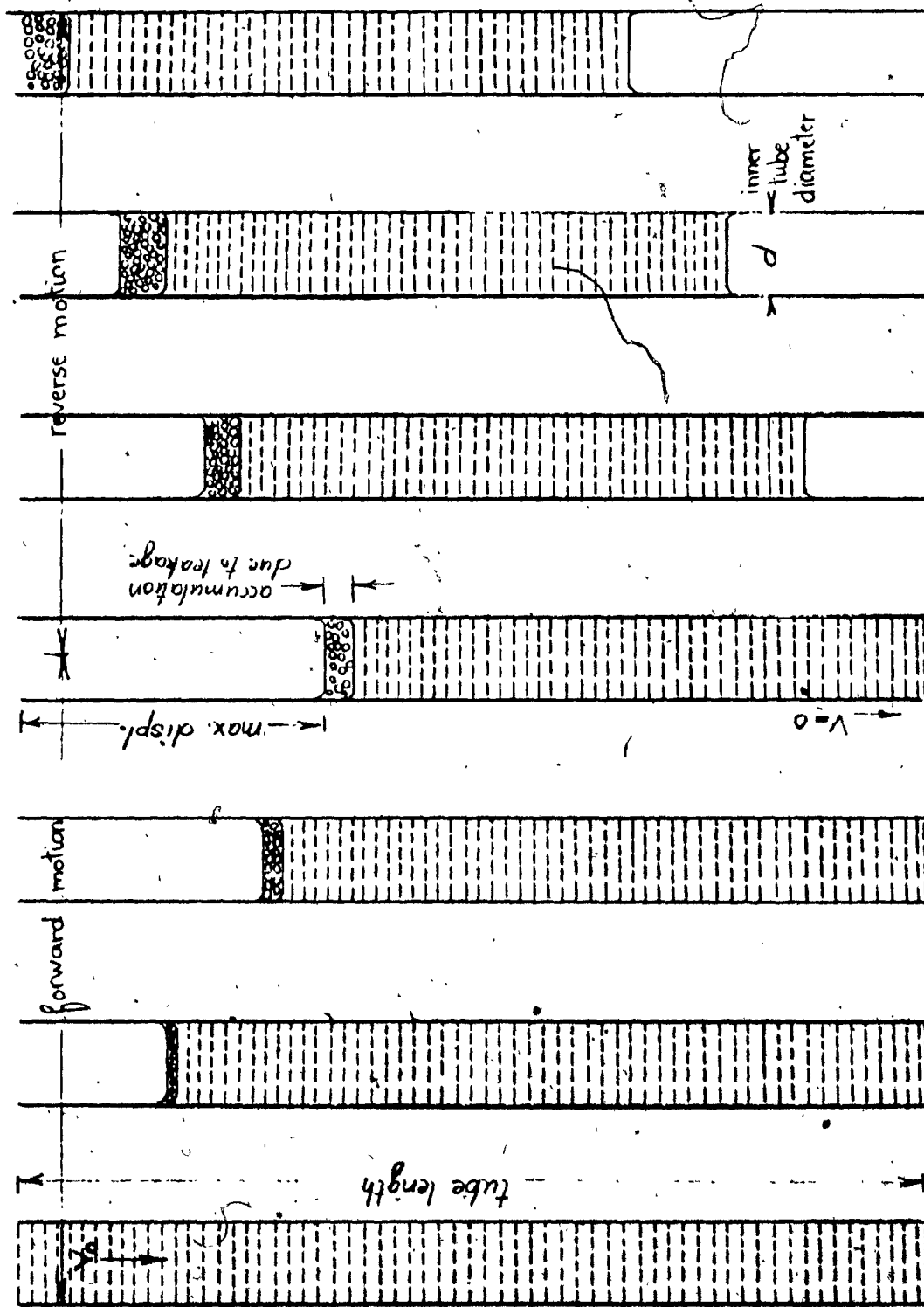
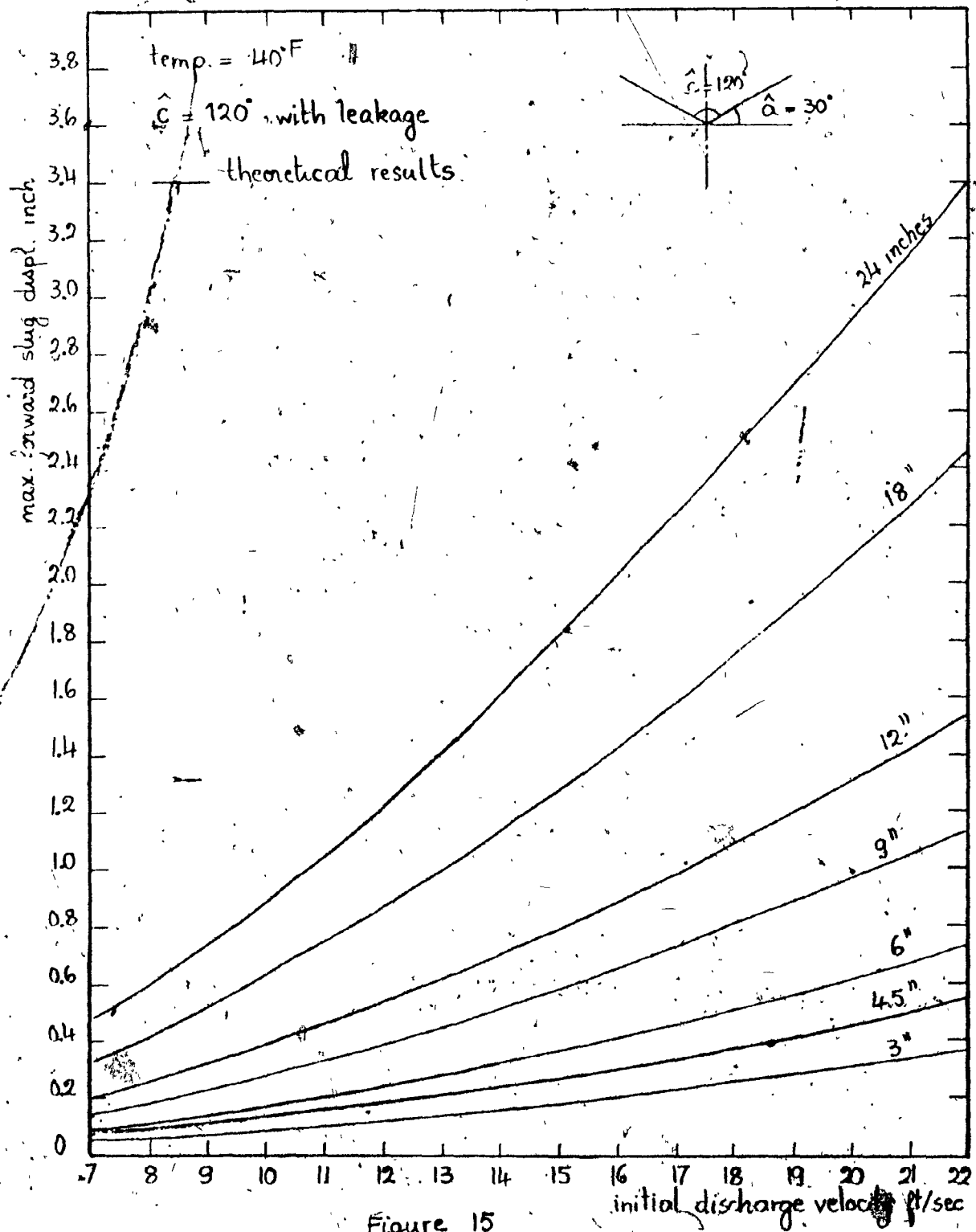


Figure 14 - Forward & reverse motion (with leakage) - (not to scale)



Relationship between max. forward slug displ. & initial discharge vel.,  $\hat{C} = 120^{\circ}$

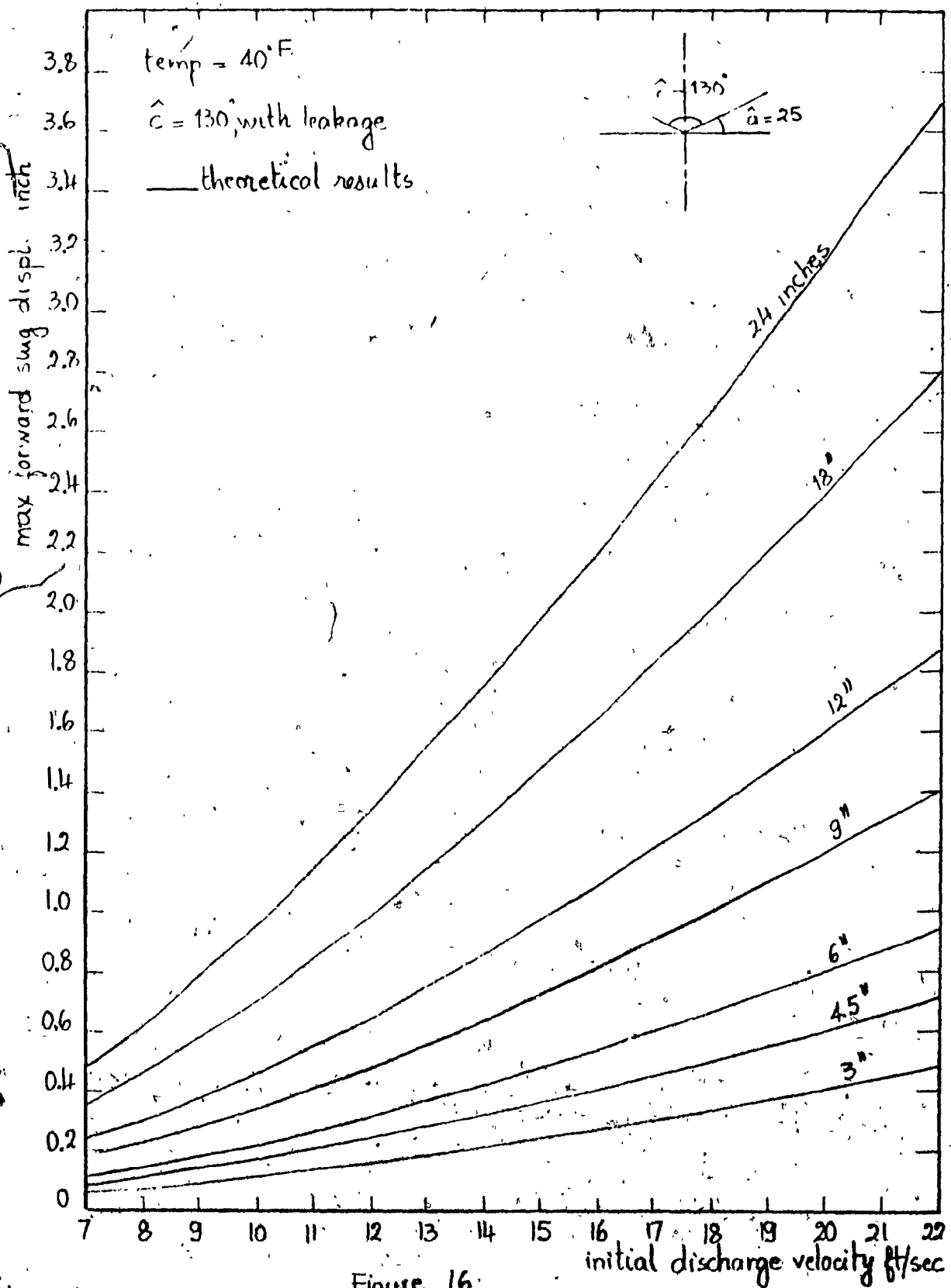


Figure 16

Relationship between max. forward slug displ. & initial discharge vel.  $\hat{c} = 130^\circ$



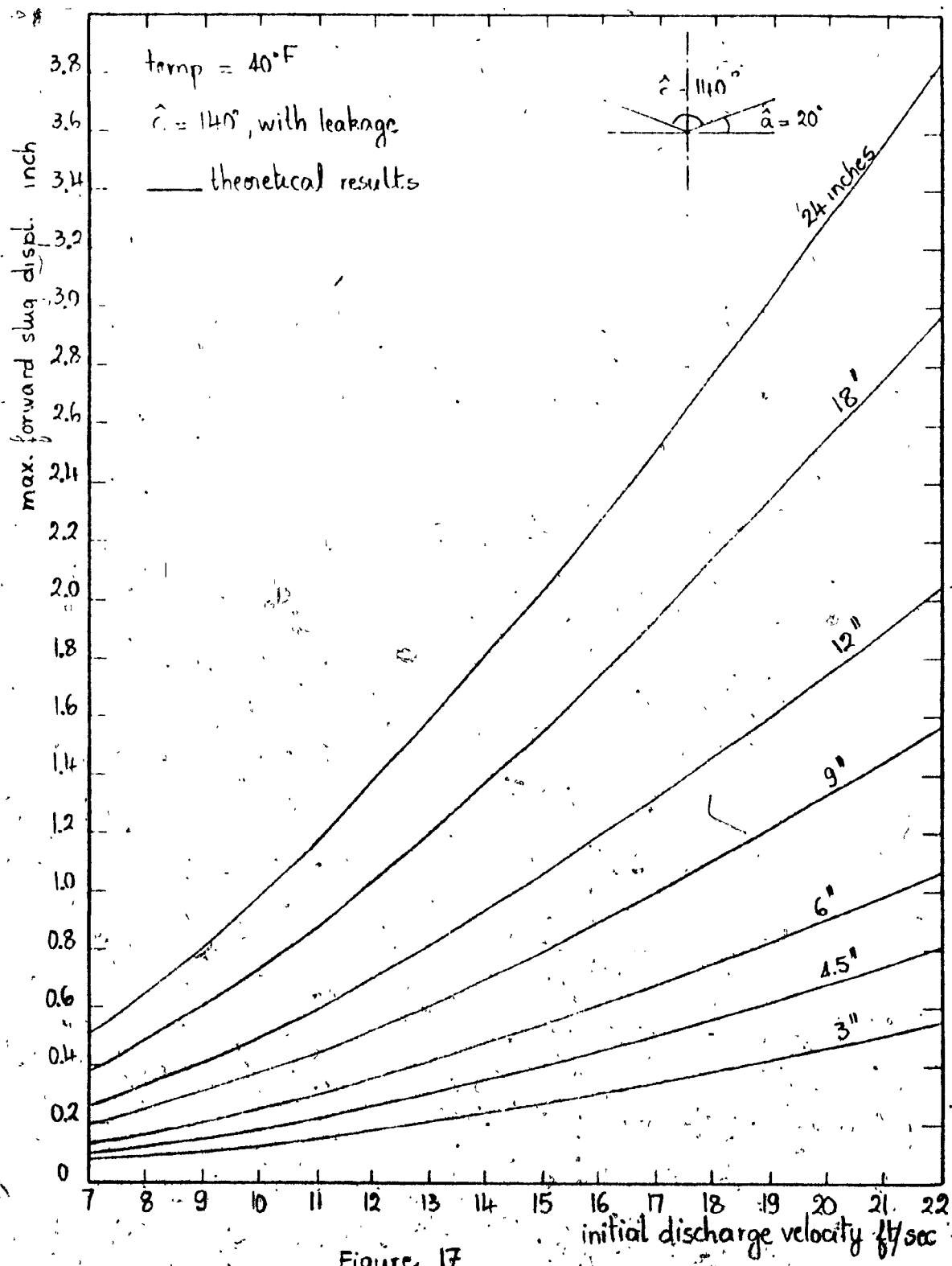


Figure 17  
 Relationship between max. forward slug displ. & initial discharge vel.  $\hat{\alpha} = 140^\circ$

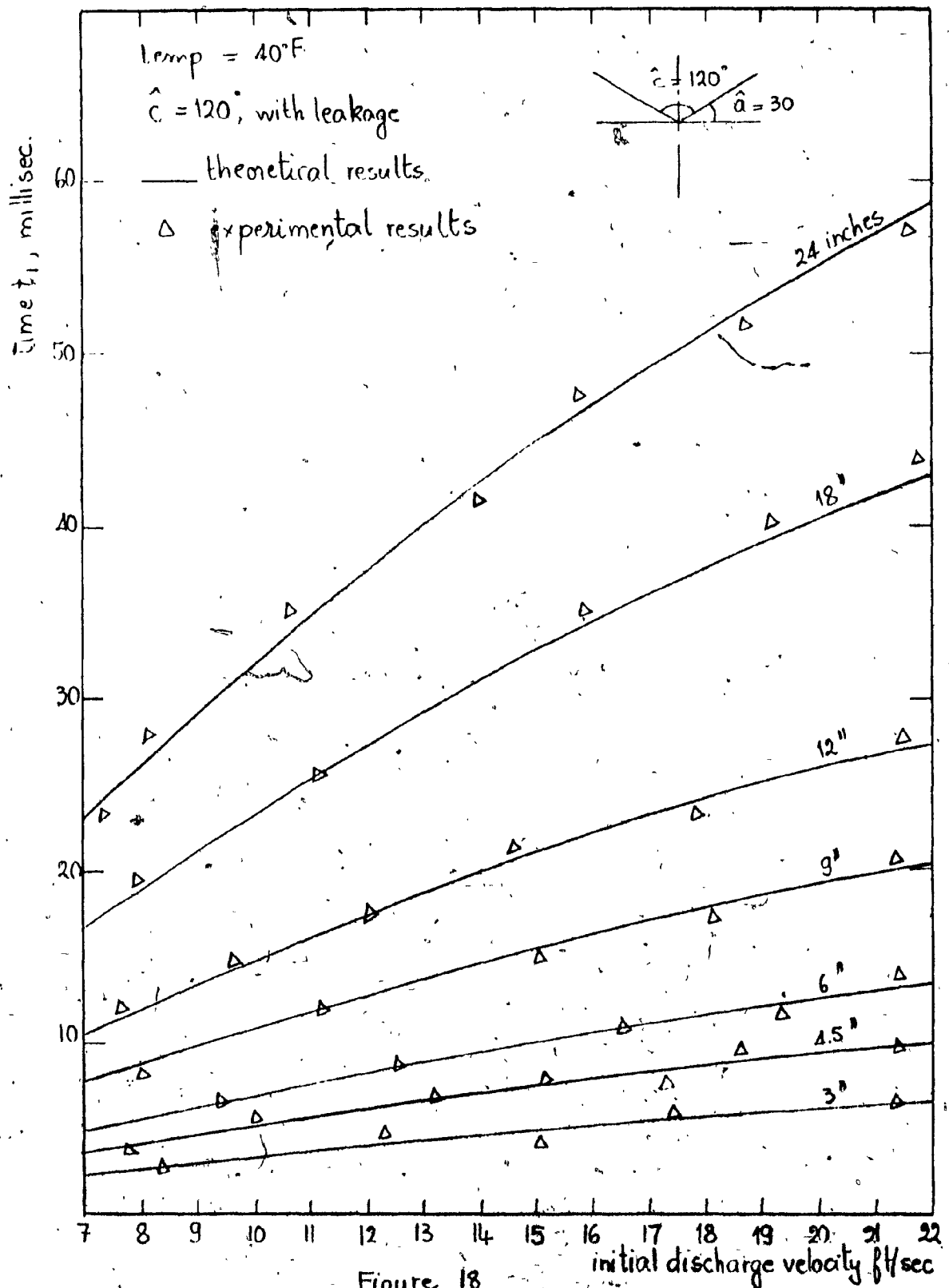


Figure 18  
 Relationship between time  $t_1$  & initial discharge velocity  $\hat{c} = 120^\circ$

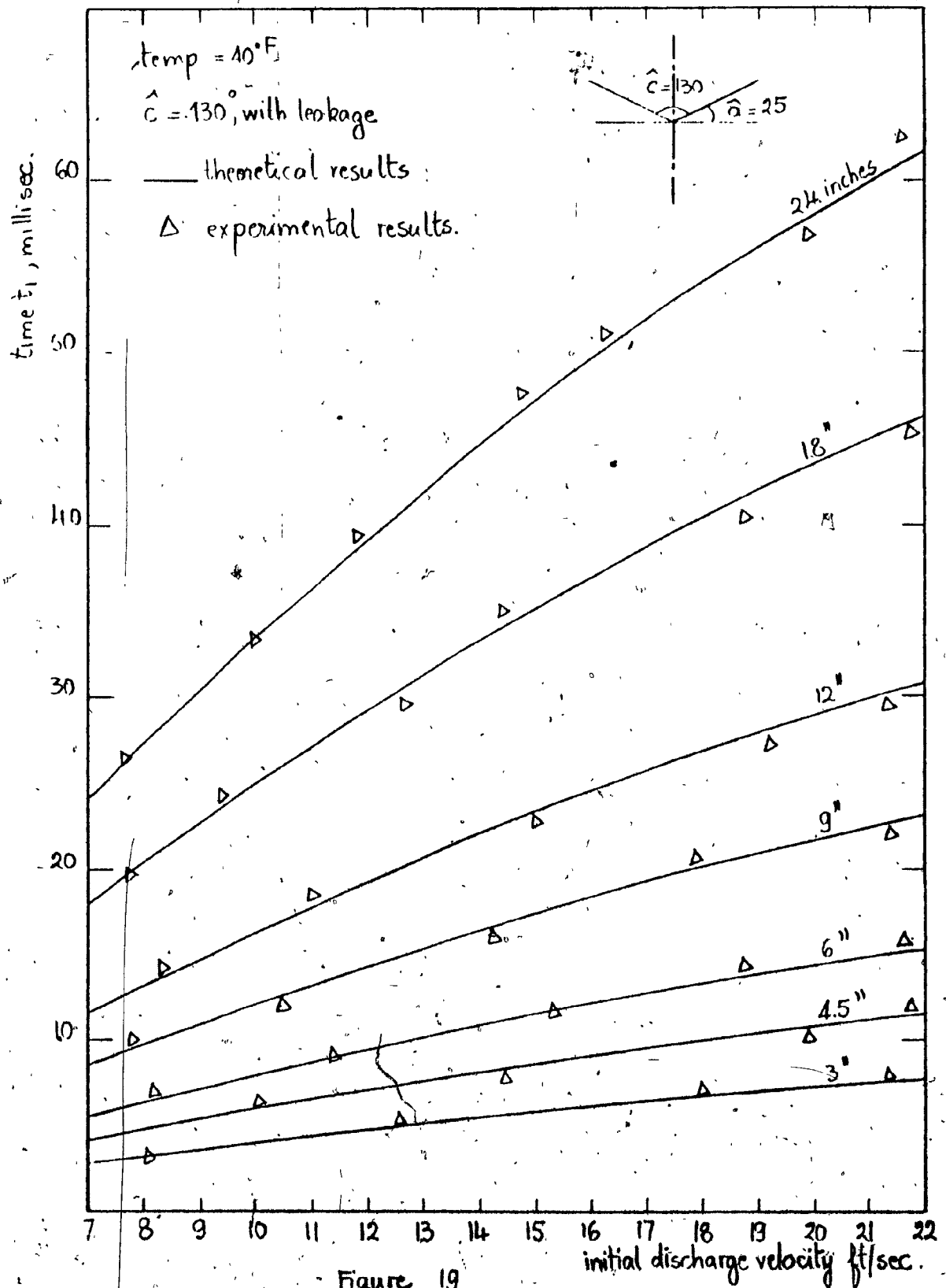


Figure 19  
 Relationship between time  $t_1$  and initial discharge velocity  $\hat{c} = 130^\circ$

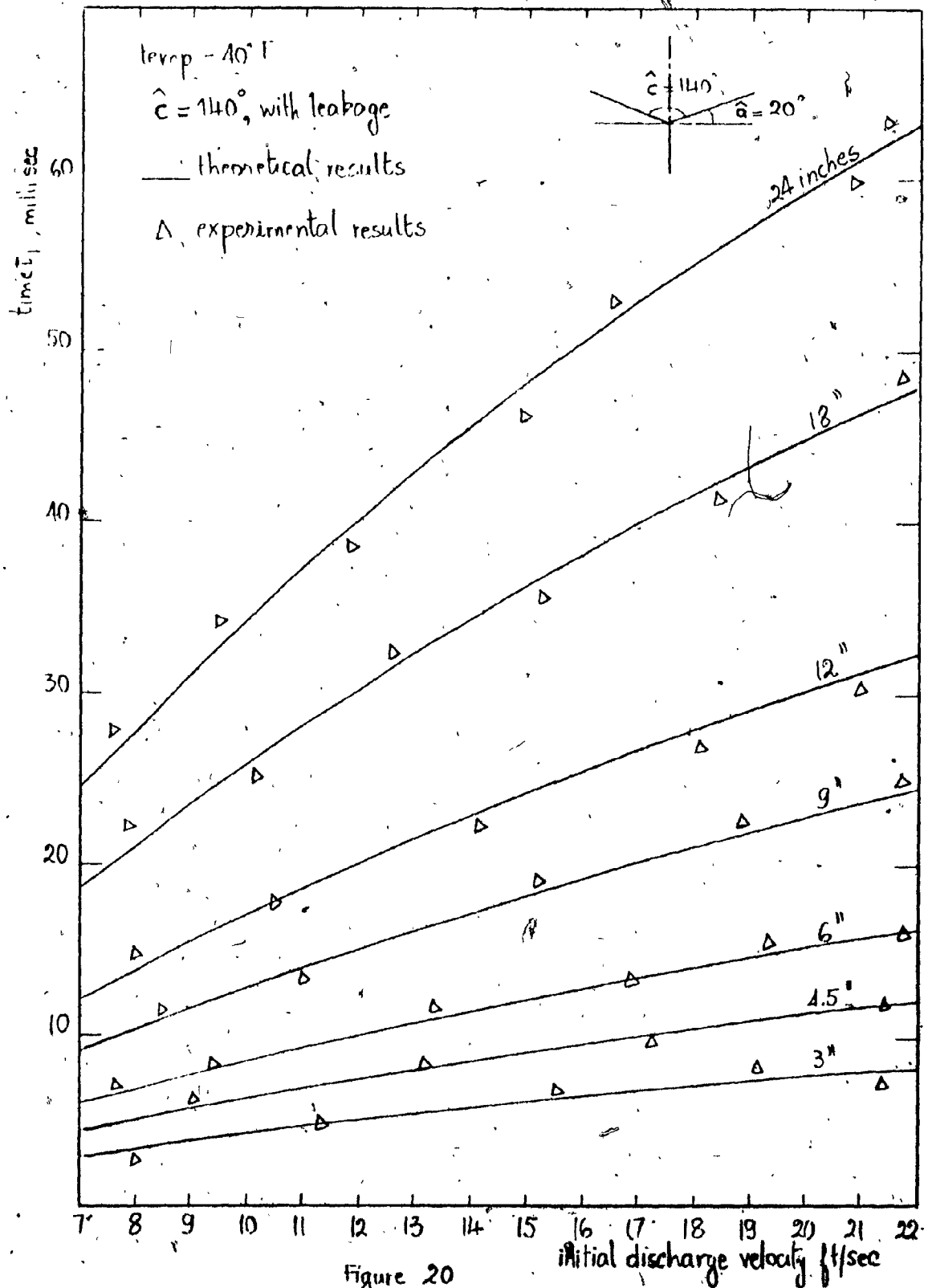


Figure 20  
 Relationship between time  $t_1$  and initial discharge velocity  $\hat{c} = 140^{\circ}$



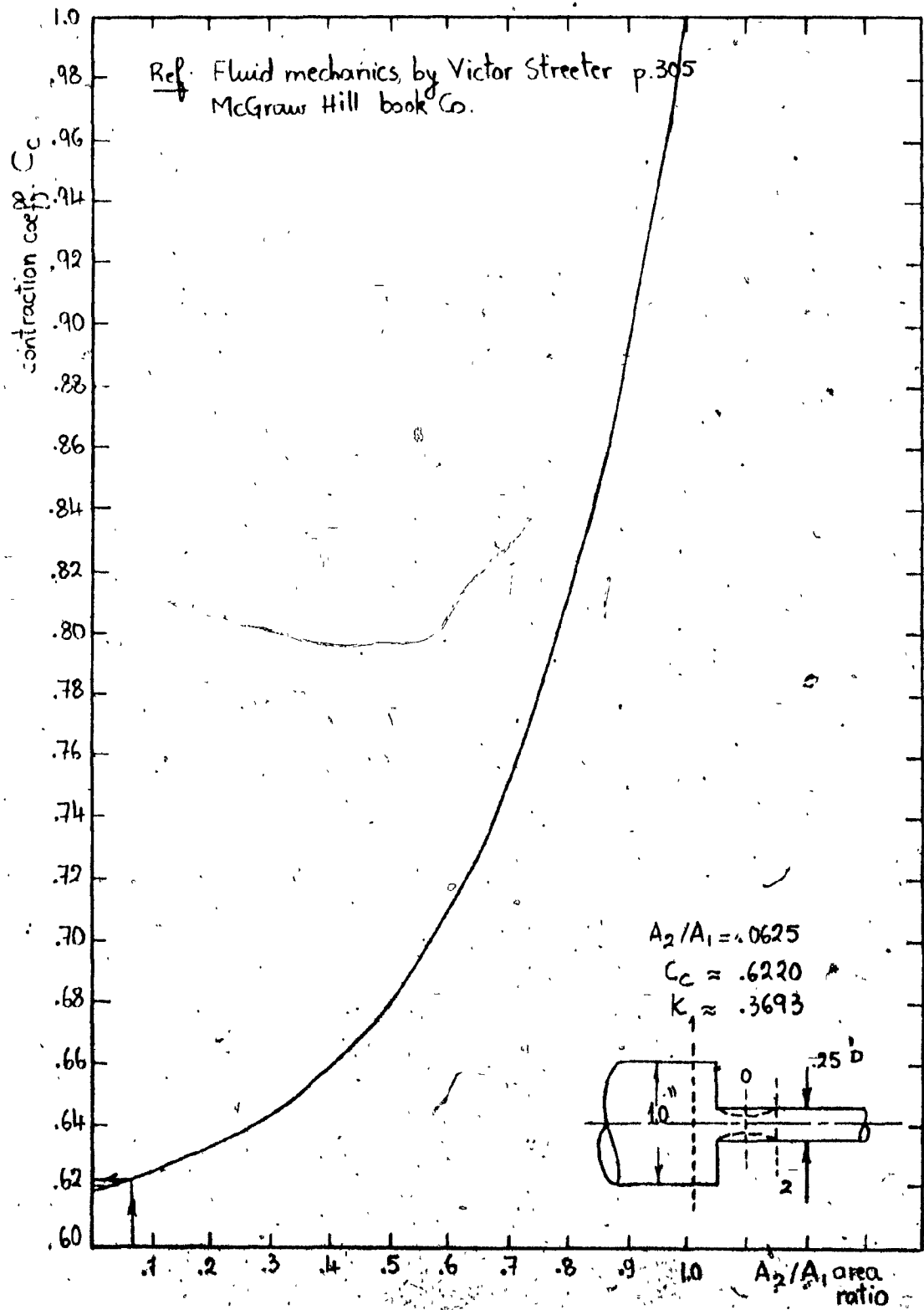


Figure 22  
Relationship between contraction coeff.  $C_c$  & area ratio

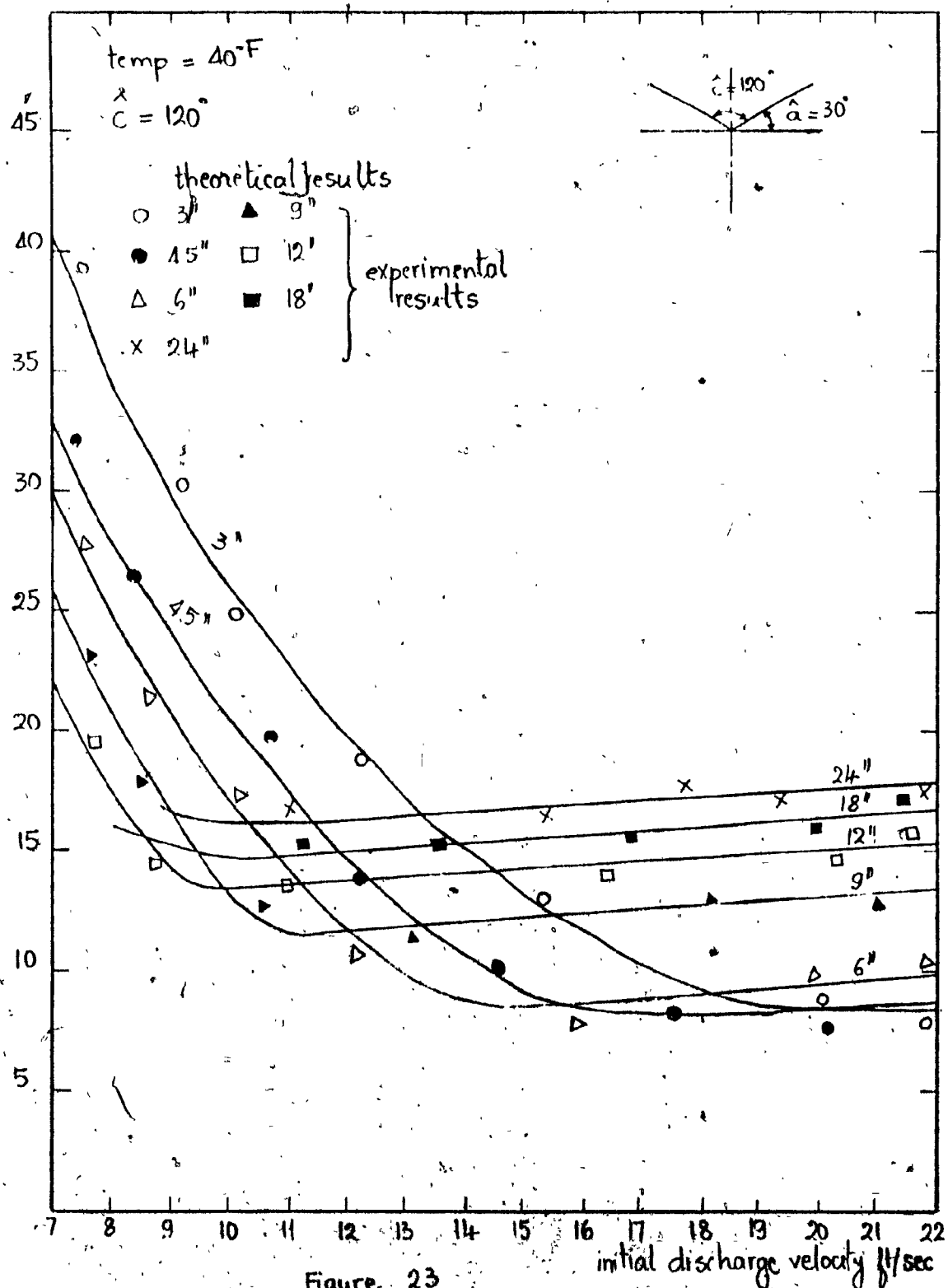


Figure 23

Relationship between time  $t_2$  & initial discharge velocity  
 (experimental & theoretical results)  $\hat{C} = 120^\circ$

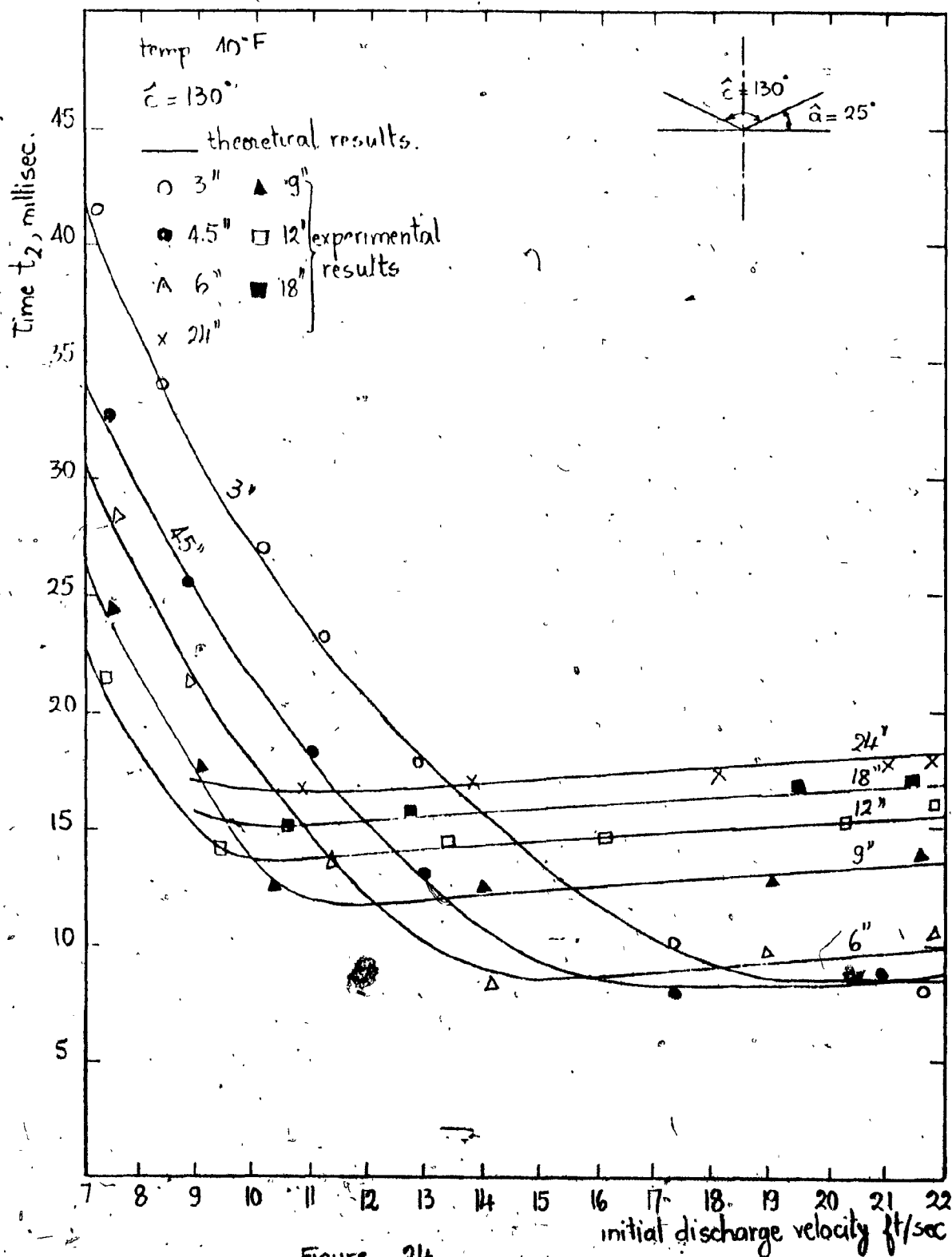


Figure 24.

Relationship between time  $t_2$  & initial discharge velocity  
 (experimental & theoretical results)

$\hat{c} = 130^\circ$



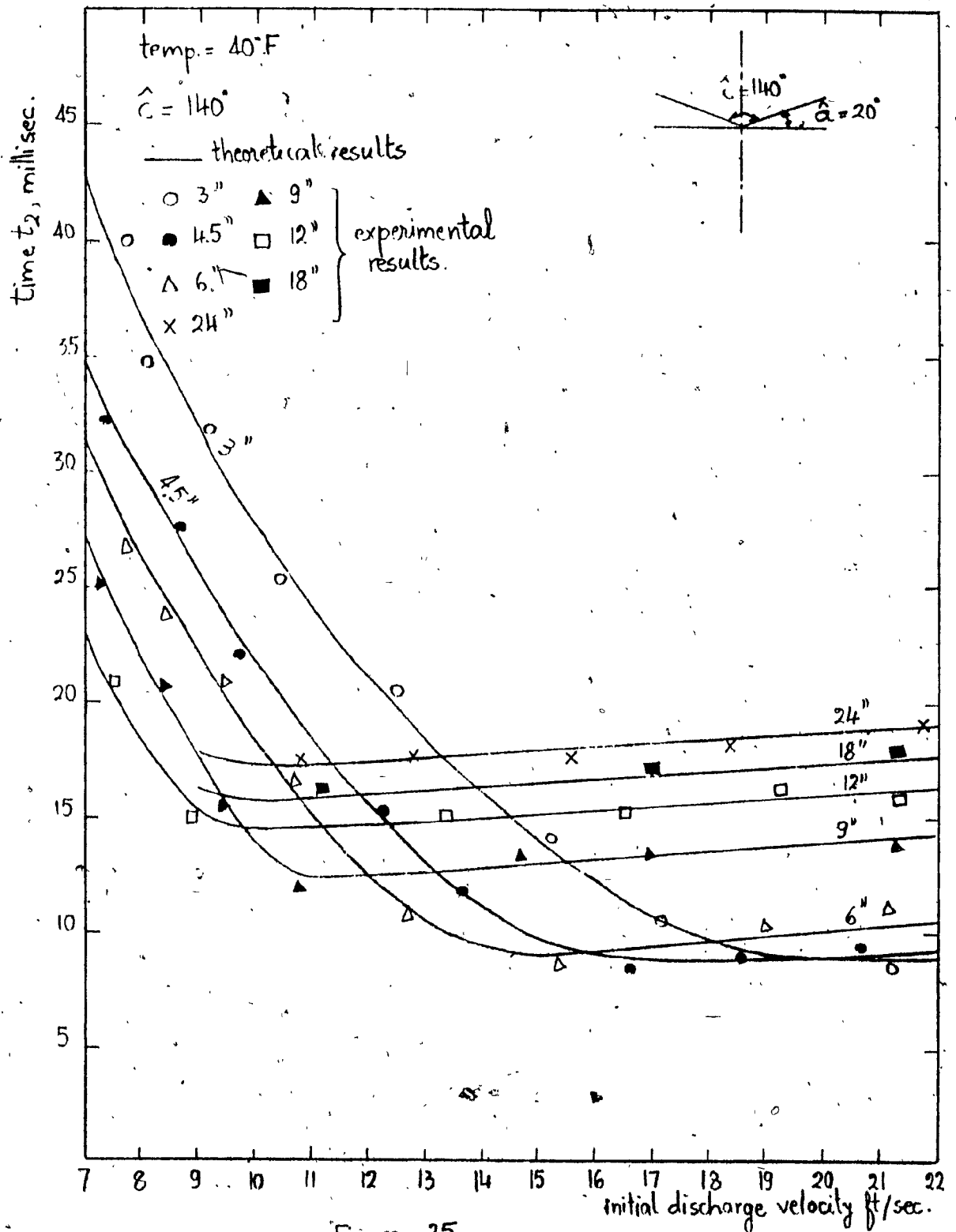
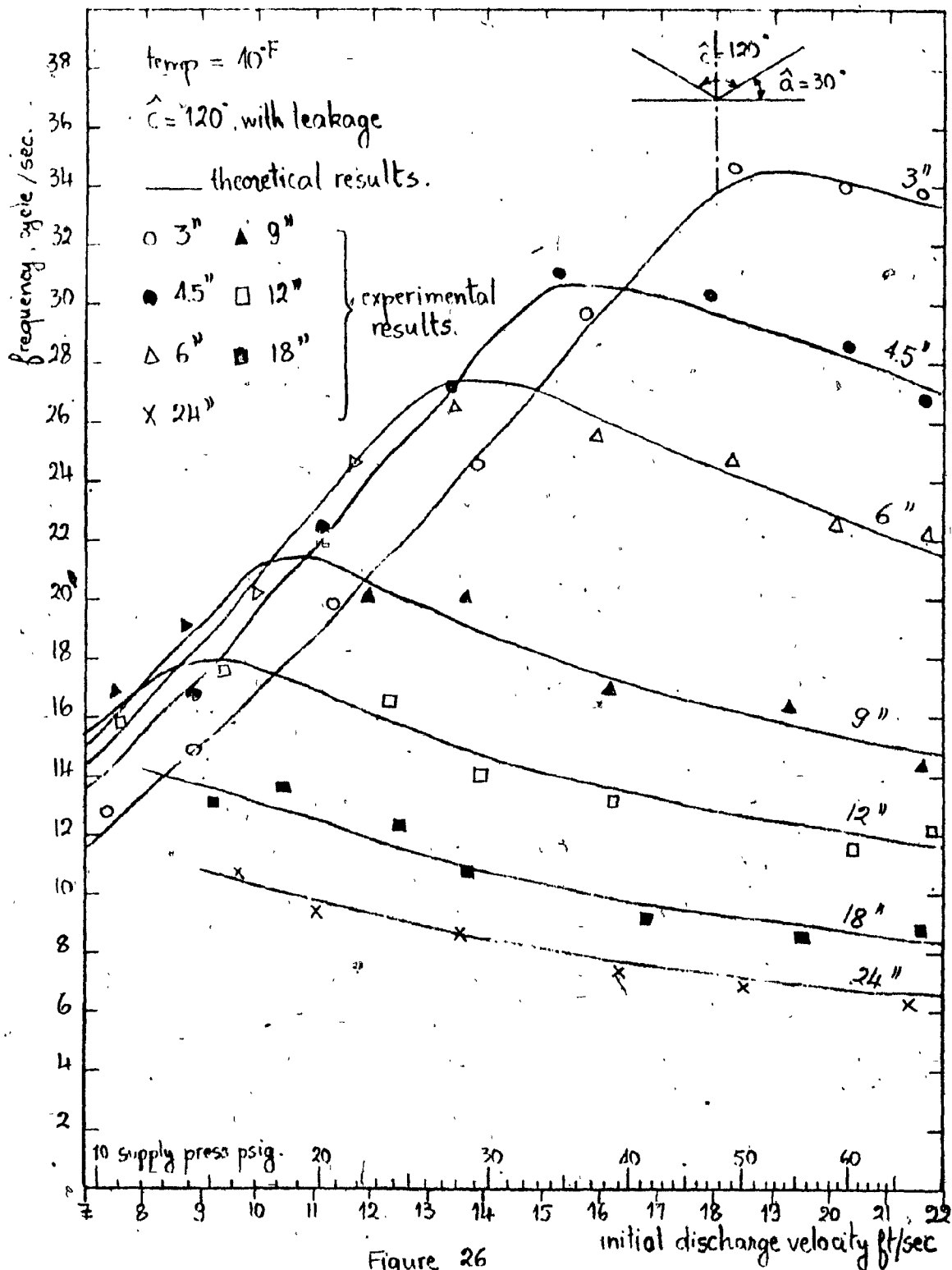


Figure 25  
 Relationship between time  $t_2$  & initial discharge velocity  
 (experimental & theoretical results)

$\hat{C} = 140^\circ$



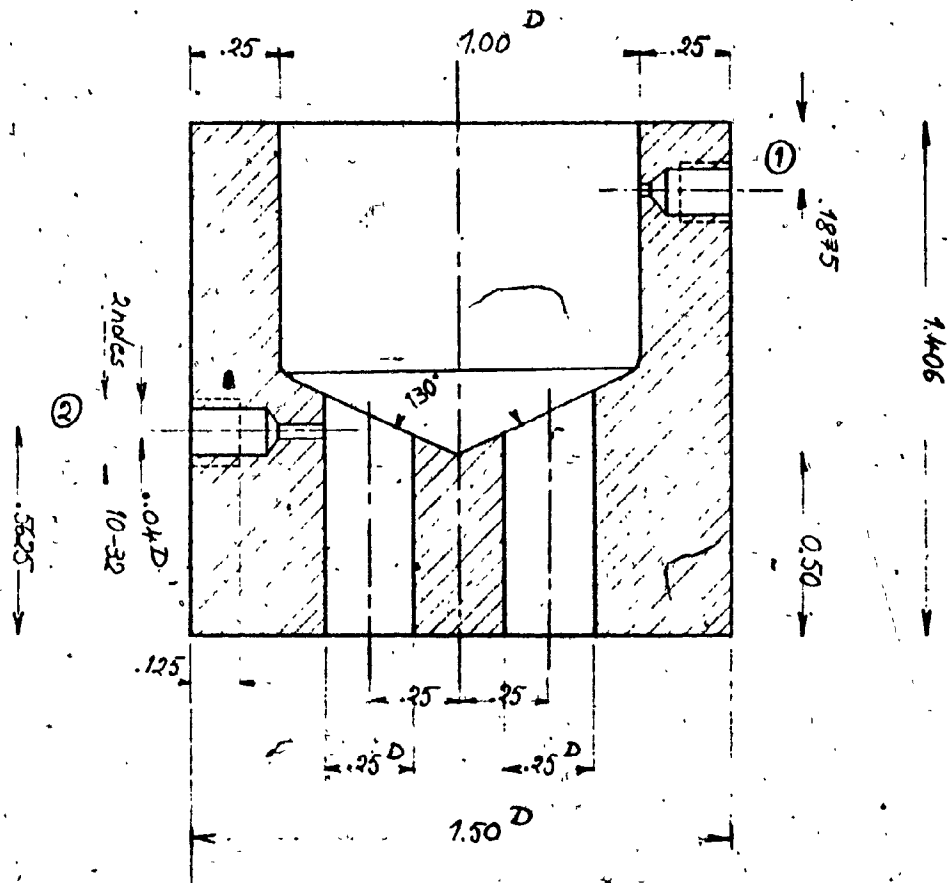


Figure 34  
Inside ball housing with  $\hat{C} = 130^\circ$

Scale: 2:1  
DIMS. IN INS.

TOLERANCES UNLESS SPECIFIED:

INCH =

.0 ± .1

.00 ± .01

.000 ± .003

METRIC:

± 0.1 mm

NAME: DRE 130

DATE:

DEC 73

NO. REQUIRED:

1

MATERIAL:

PLEXI

DESIGNED BY:

YHAGGAG

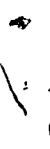
SCALE:

2:1

CONCORDIA UNIVERSITY  
FLUID CONTROL CENTER

NUMBER:

IV



8

Scale 2:1

CONCORDIA UNIVERSITY  
FLUID CONTROL CENTER  
NUMBER: VI

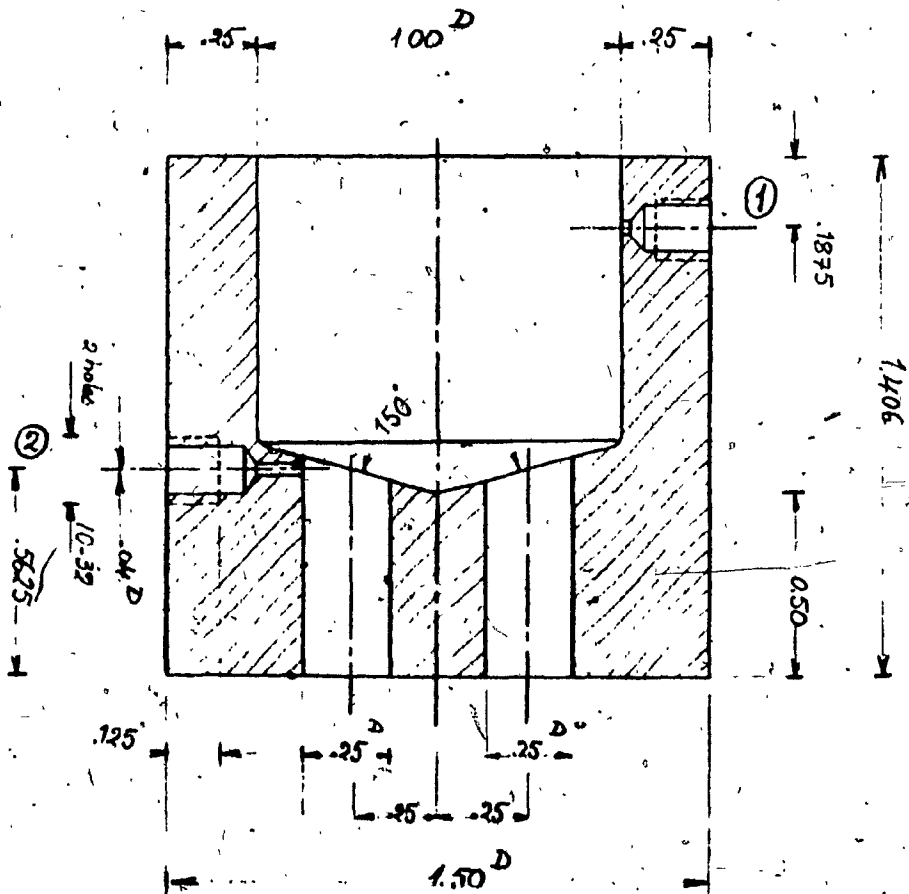


Figure 36  
Inside ball housing with  $\hat{C} = 150^\circ$

Scale 2:1  
DIMS. IN INS.

TOLERANCES UNLESS SPECIFIED:			
INCH =		METRIC:	
.0	± .1		± 0.1 mm
.00	± .01		
.000	± .003		
NAME: CORE 150		DATE: DEC 75	NO. REQUIRED: 1
MATERIAL: PLEXT		DESIGNED BY: YHAGSAG	SCALE: 2:1
CONCORDIA UNIVERSITY			
FLUID CONTROL CENTER			
NUMBER: VII			

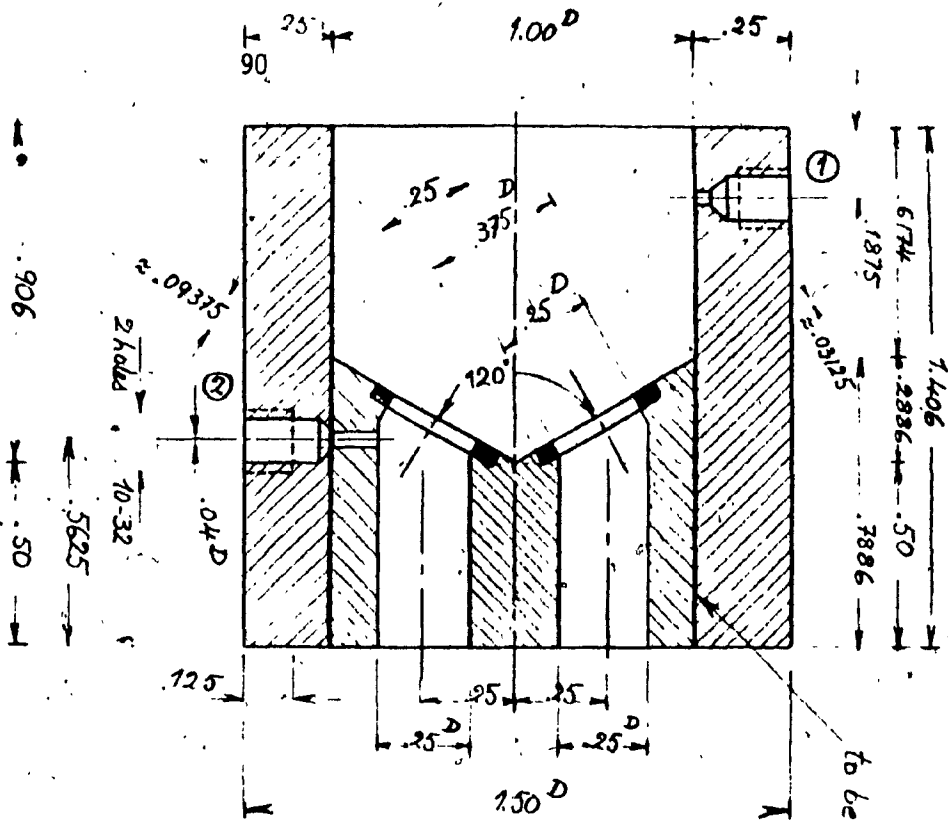
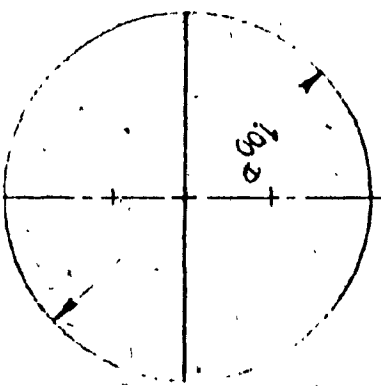
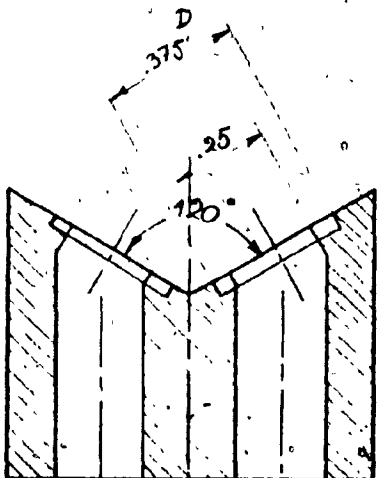


Figure 37  
No-leakage inside ball-housing  
Scale 2:1  
DIMS. IN INS.



TOLERANCES UNLESS SPECIFIED:		NAME:		DATE:		NO. REQUIRED:		CONCORDIA UNIVERSITY	
INCH =		CORE 120-2		DEC 75		1		FLUID CONTROL CENTER	
.0 ± .1		MATERIAL:		DESIGNED BY:		SCALE:		NUMBER:	
.00 ± .01		PLEXT		YHAGGAG		2:1		IX	
.000 ± .003									

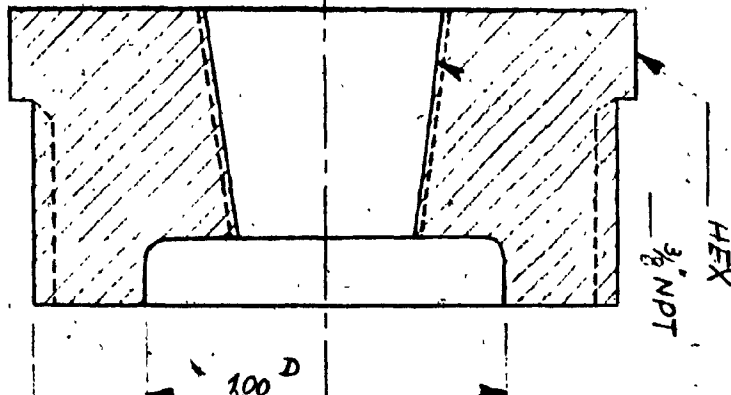


Figure 38  
Locking Nut,

Scale 2:1  
DIMS. IN INS.

TOLERANCES UNLESS SPECIFIED:

INCH =  
0 ± .1  
.00 ± .01  
.000 ± .003

METRIC:  
± 0.1 mm

NAME:

NUT

MATERIAL:

BRASS

DATE:

DEC 75

DESIGNED BY:

YHAGGAG

NO. REQUIRED:

1

SCALE:

2:1

CONCORDIA UNIVERSITY

FLUID CONTROL CENTER

NUMBER:

XVII

TOLERANCES UNLESS SPECIFIED:		NAME:	DATE:	NO. REQUIRED:	CONCORDIA UNIVERSITY FLUID CONTROL CENTER
INCH =	METRIC:	MATERIAL:	DESIGNED BY:	SCALE:	
.0 ± .1	± 0.1 mm	PLEXI	DEC 75	1:1	NUMBER: <u>XIV</u>
.00 ± .01					
.000 ± .003					

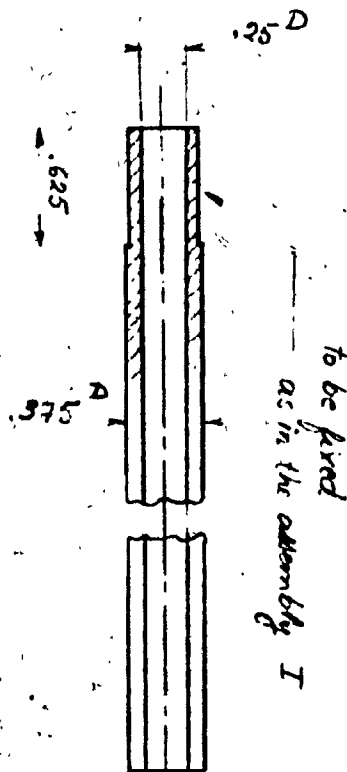


Figure 39  
different tube length

Scale 1:1

DIMS. IN INS.

Inside diam. .25"

Outside diam. .375"

Couple of tube length:

3.625" - 6.625" - 9.625"

15.625" - 21.625"



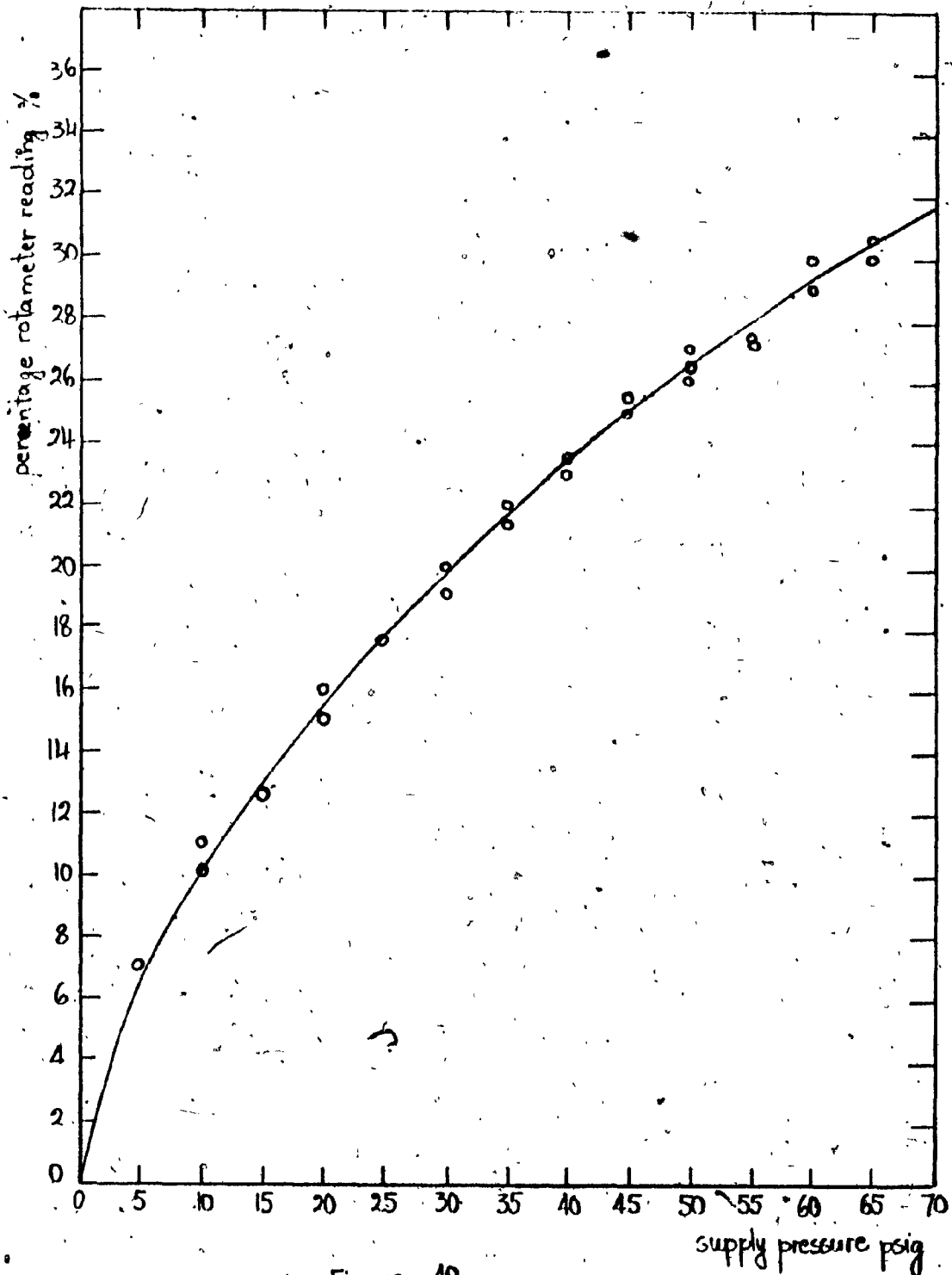


Figure 40  
Experimental results between the supply pressure and the percentage  
rotameter readings (max. flow rate = 21.6 USGPM ; 1 USG = 231 in<sup>3</sup>)

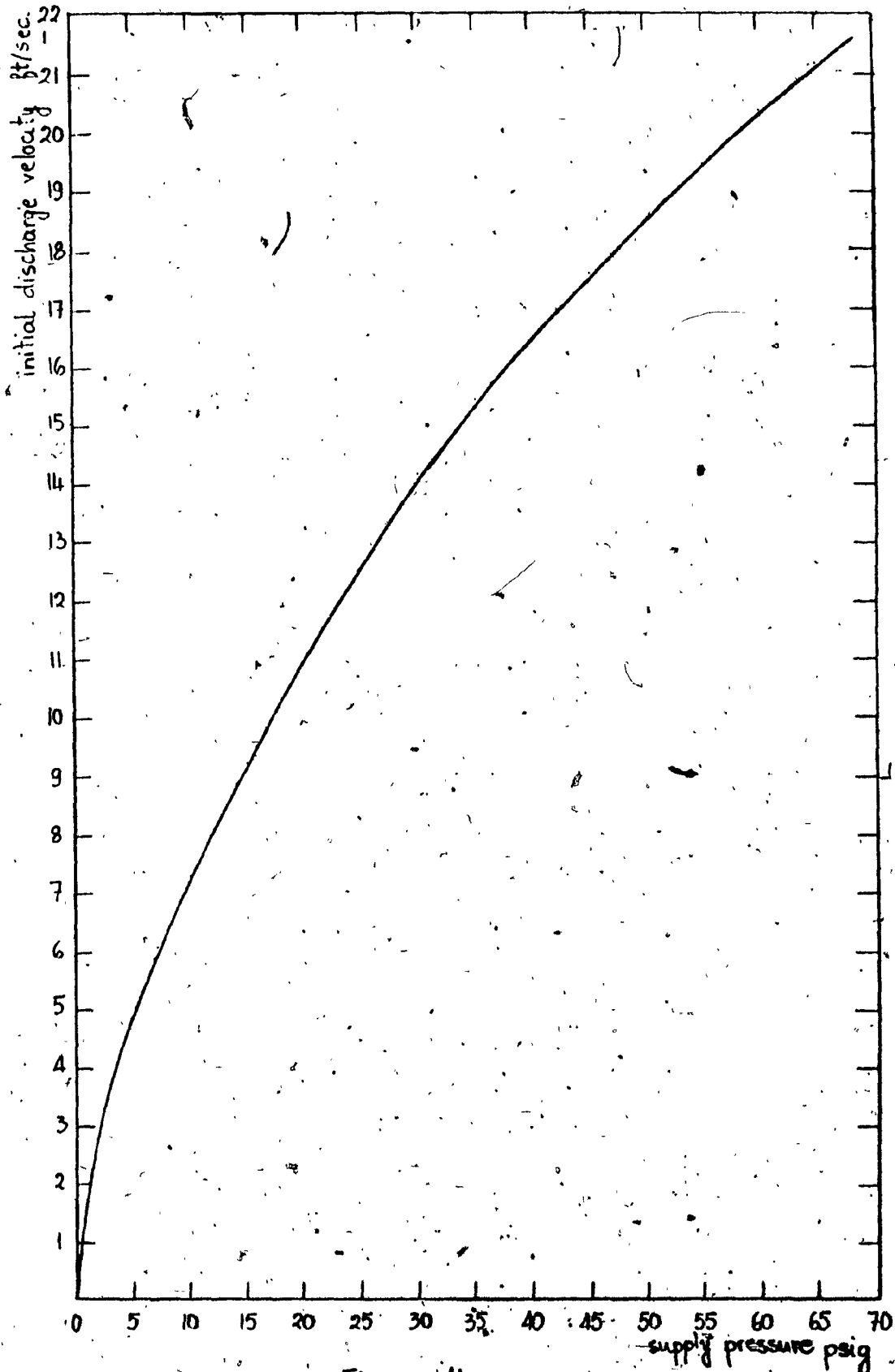
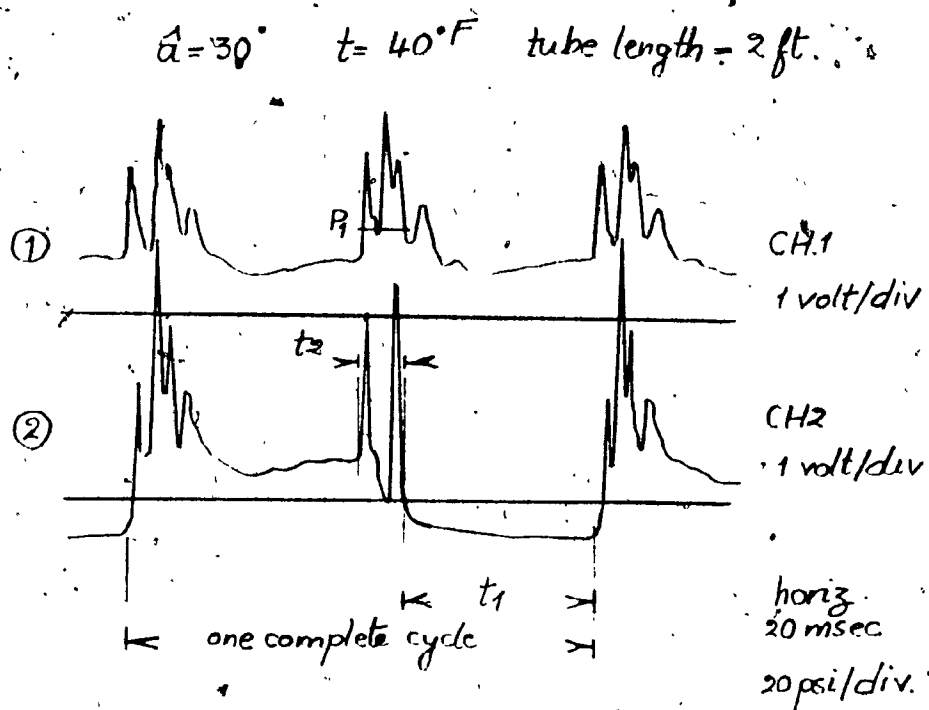


Figure 41  
calculated initial discharge velocity versus the corresponding supply pressure.



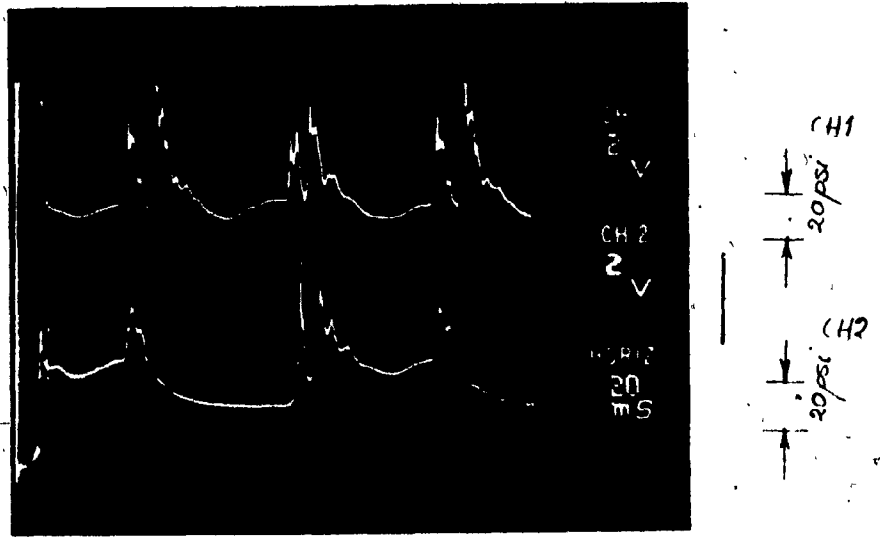
supply pressure  $\approx 65$  psig  
 discharge velocity  $\approx 21$  ft/sec  
 with leakage

$$t_2 \approx 16 \text{ msec}$$

$$t_1 \approx 57 \text{ msec}$$

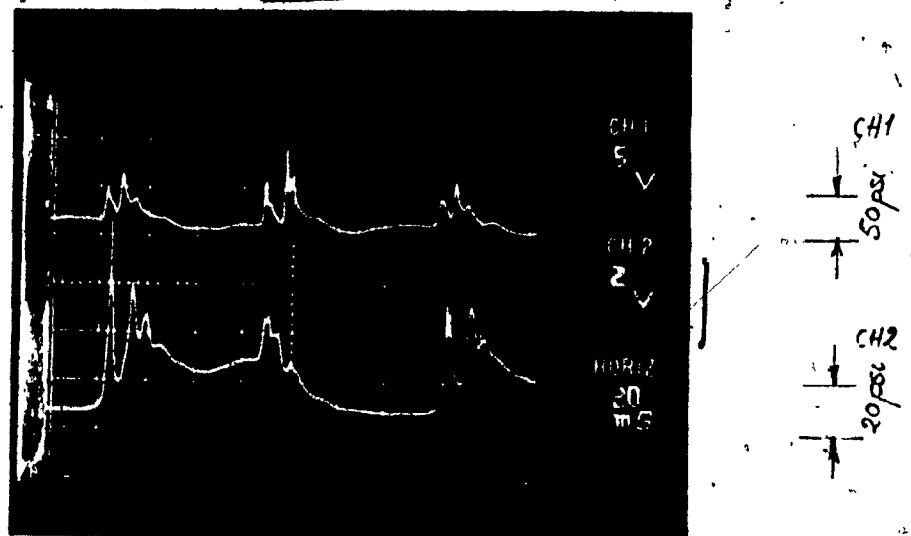
$$\text{frequency} \approx 6.84 \text{ cycle/sec}$$

Figure 42. = Typical pressure distribution



$P_{supply} = 30 \text{ psig}$  ;  $L = 2 \text{ ft}$  ; without linkage.

Figure 43



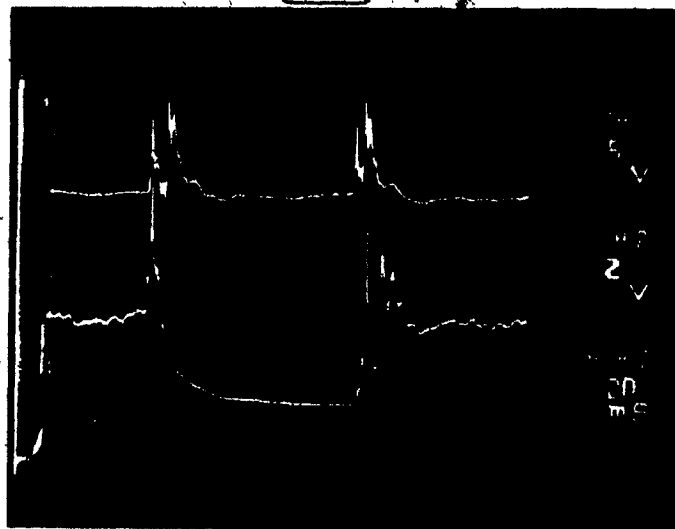
$P_{supply} = 30 \text{ psig}$  ;  $L = 2 \text{ ft}$  ; without linkage

Figure 44



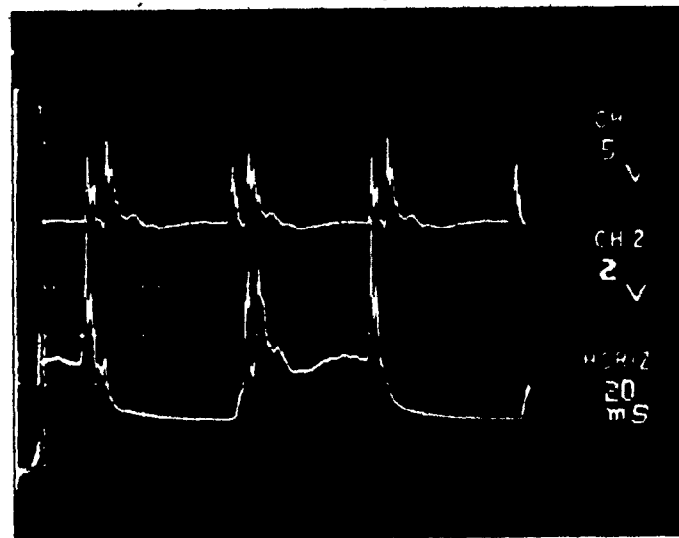
$P_{supply} = 45 \text{ psig}$  ;  $L = 2 \text{ ft}$  ; without leakage

Figure 45



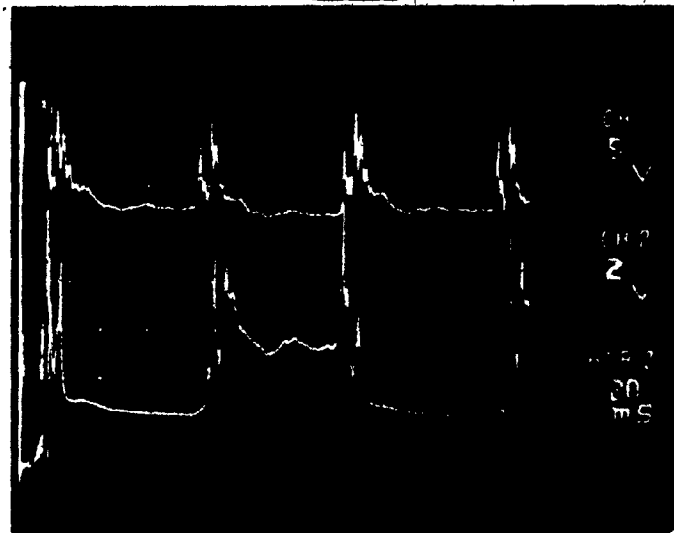
$P_{supply} = 66 \text{ psig}$  ;  $L = 2 \text{ ft}$  ; without leakage

Figure 46



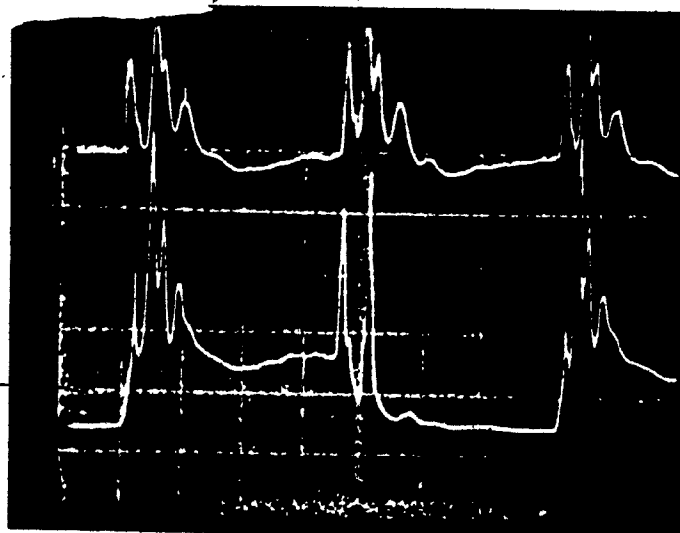
$P_{supply} = 35 \text{ psig}$ ;  $L = 18 \text{ inches}$ ; without leakage

Figure A7



$P_{supply} = 65 \text{ psig}$ ;  $L = 18 \text{ inches}$ ; without leakage

Figure A8



CH1  
20 psi  
CH2  
20 psi  
Horiz  
20 ms

$P_{supply} = 65 \text{ psig}$  ;  $L = 2 \text{ ft}$  ; with leakage,  $\hat{a} = 30^\circ$

Figure 49



CH1  
20 psi  
CH2  
20 psi  
Horiz  
20 ms

$P_{supply} = 60 \text{ psig}$  ;  $L = 2 \text{ ft}$  ; with leakage,  $\hat{a} = 30^\circ$

Figure 50

## APPENDIX A

MIMIC program for the solution of the forward and reverse  
slug motion equations



C CONCORDIA UNIVERSITY - MECHANICAL ENGINEERING DEPT.  
 C DR. GEORGE WELSH, CHAIRMAN - MUNICIPAL  
 C FLUID CONTROL CENTER - WALL OSCILLATOR PROJECT  
 C STUDY OF THE SLUG DYNAMICS

		CONCDA, HETA)	
		PARUM1, PSS, COI	FT/SEC
	DT	0.031	
		INITIAL VELOCITY	
C	UO	12.001	INCH/SEC
		TUBE LENGTH	
C	L	12.00	INCH
		TUBE DIAMETER	
C	D	0.250	INCH
	AREA	3.14159*0.074*(12.00*12.00)	FT2
		FEED WATER TEMPERATURE	
C	TEMP	40.00	OF
	TEMPA	TEMP*460.0	R
		SPECIFIC WEIGHT	
C	RHO	62.426	LB/FT3
	RHOVAP	0.0040	LB/FT3
		VAPOR PRESSURE	
C	PV	0.12163	LB/IN2A
		KINEMATIC VISCOSITY	
C	KVISC	1.66*PWR(10.0, -5.0)	FT2/SEC
		PEYHOLD NUMBER	
C	PENUM	ARG(XD)*0.0/(144.0*KVISC)	
	K	144.0*144.0*32.174	
	KK	2.0*RHOVAP*32.174*144.0	
	RAIR	53.350*12.0	

		DETERMINATION OF THE FRICTION FACTOR REGIONS	
	K1	640.00	
	K2	2000.0	
	K3	PWR(10.0, 5.0)	
	LK1	FSWIRENUM-K1, TRUE, FALSE, FALSE)	
	LK2	FSWIRENUM-K2, TRUE, FALSE, FALSE)	
	LK3	FSWIRENUM-K3, TRUE, FALSE, FALSE)	
	GEK1	NOT(LK1)	
	GEK2	NOT(LK2)	
	GEK3	NOT(LK3)	
	K1K2	AND(GEK1, LK2)	
	K2K3	AND(GEK2, LK3)	
LK1	FFF	64.0/(IRENUM*0.00001)	
K1K2	FFF	64.0/IRENUM	
K2K3	FFF	0.3164/0.25R	
GEK3	FFF	0.184/0.2R	
	FF	FFF	
	CC25R	0.25*LOG(IRENUM)	
	025R	EXP(L025R)	
	LC2R	0.2*LOG(IRENUM)	
	02R	EXP(L02R)	

		CALCULATION OF THE LEAKAGE EFFECT	
		ANGLE OF INNER CORE	
	A	30.0*3.1416/180.0	
	CCC	11.0-COS(A)/COS(A)	
	DPRESS	PSS-PC	
	VACC	C(30.0*(K1+DPRESS)/LEVELDENSITY	10/IN2A
	ACCUM	T*VACC*12.0	FT/SEC COMPUTER CENTER
	XREAL1	X-ACCUM	INCH

		SOLUTION OF THE DIFFERENTIAL EQUATIONS	
		OSCILLATOR INCLINATION WITH THE VERTICAL AXIS	
	B	0.0*3.1416/180.0	
	XO	INT(XCO, UO)	INCH/SEC
	X	INT(XD, 0.0)	INCH
	OK1	FSW(XD, FALSE, TRUE, TRUE)	
OK1	X1	X	
OK1	T1	T	
	OK2	NOT(OK1)	
		PRESSURE INSIDE THE CAVITY	
C	PC	PV+PAIR	10/IN2A
		EFFECT OF DISSOLVED AIR	
OK1	PAIR	DETA*T*RAIR*TEMPA/(144.0*AREA*(X*0.00001))	10/IN2A
OK2	PAIR	DETA*T1*RAIR*TEMPA/(144.0*AREA*(X*0.00001))	10/IN2A
OK1	BALL	K*(PC-PAI)/(RHO*(L-X))-FF*XO*XO/(2.0*DI*386.088*COS(9))	IN/SEC2
OK2	BALL	K*(PC-PAI)/(RHO*(L-X1))-FF*XO*XO/(2.0*DI*386.088*COS(9))	IN/SEC2
	XO	BALL	IN/SEC2
OK1	X2	C.CO	
OK2	X2	FSW(X, 100.0, 100.0, -10.0)	
		FIN(X2, 10.0)	

		HEADING, PRINTING AND PLOTTING	
		HOR(TIME, DISPL., DISPL., VELOC., F.FAC., PENUM.)	
		HOR	
		OUTLET, X, XREAL1, XO, FF, PENUM)	
		PLOT, X, XREAL1, XO, FF, PENUM)	
		END	

## APPENDIX B

FORTRAN program for the solution of the mathematical model